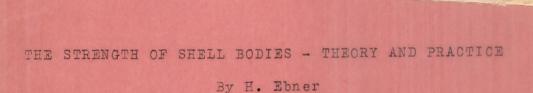
TECHNICAL MEMORANDUMS

63

NATIONAL ADVISORY COMMITTEE FOR AERONAUTICS

NAOA-TM-838

No. 838



Luftfahrtforschung Vol. 14, No. 3, March 20, 1937 Verlag von R. Oldenbourg, München und Berlin

> Washington September 1937

NATIONAL TECHNICAL
INFORMATION SERVICE
U. S. DEPARTMENT OF COMMERCE
SPRINGFIELD, VA. 22161

### NATIONAL ADVISORY COMMITTEE FOR AERONAUTICS

TECHNICAL MEMORANDUM NO. 838

THE STRENGTH OF SHELL BODIES - THEORY AND PRACTICE\*

By H. Ebner

The monocoque form of construction characterized by the fact that the skin is made as much as possible a stress-bearing member, has become increasingly popular, especially in the fuselages of the latest metal airplanes. It has introduced a number of new problems to the stress calculator and the designer.\*\* The problems for the stress calculator fall into two groups: The determination of the stress condition (shell statics) and the determination of the failing strength (shell strength). A large part of these problems may, as a result of the research work of the last few years, be looked upon as being solved. The present report summarizes the most important theoretical and experimental results on this subject, special attention being given to the work done at the German Research Laboratory for Aeronautics (DVL).

I. INTRODUCTION

REPRODUCED BY
NATIONAL TECHNICAL
INFORMATION SERVICE
U.S. DEPARTMENT OF COMMERCE
SPRINGFIELD, VA. 22161

Designs of Shell Bodies

In order to gain a comprehensive concept of the systems discussed in the following, a survey is made of the various forms of construction of shell bodies as developed in Germany. The departures in the individual designs are less the result of differences of opinion as to what constitutes the best design from the point of view of strength and stiffness than the considerations of simple manufacture, upkeep, and repair possibilities; aside from that the design is governed by aerodynamic requirements, the necessity of cutaway sections, installations, etc.

Most shell bodies consist of a structure of stiffeners and bulkheads to which the metal skin is riveted. The characteristic of the shell body is that the skin actually

<sup>\*&</sup>quot;Theorie und Versuche zur Festigkeit von Schalenrumpfen."
Luftfahrtforschung, vol. 14, no. 3, March 20, 1937.

<sup>\*\*</sup> For a survey of these problems, see Luftwissen, December 1935.

participates as much as possible in the stress bearing. This may be accomplished either with a skin thick enough by itself for all stresses or with a correspondingly thin skin in conjunction with a system of stiffeners. Shell bodies without stiffeners of any kind or such with bulkheads only, are rare; such bodies would have to be so designed that the skin does not buckle up to the failing load. Contrariwise, body shells with stiffeners and bulkheads may be designed with buckling-resistant skin or with a skin which buckles before the failing load is reached. The suitability of either arrangement depends upon the circumferential loading defined by the structural height, the loading of the body, and upon the curvature of the skin.

A special case of shell body is that where only longitudinal flanges at a few - four at the most - points provide for the longitudinal stresses, while the stiffeners in between serve only to reinforce the skin but not to take up stress. In that case the skin primarily serves to carry shear stresses.

The following contains a brief outline of various German shell-design practices. Heinkel and Henschel employ stiffeners and bulkheads of open Z-sections or . Uchannels (figs. 1 and 2). The continuous stiffeners are fairly evenly distributed over the circumference in the central and rear portion of the body, but spaced somewhat closer in the zones of greater compression stresses. bulkheads are joined to the inside edge of the stiffeners without touching the skin. In the forebody, where the bulkheads are necessary for the load introduction and the inside space must be utilized to the fullest advantage, the bulkheads rest on the skin (fig. 3). In view of the generally existing cutaway sections, the axial loads here are carried in four concentrated flanges; the intermediate stiffeners merely serve as reinforcement and are interrupted at the bulkheads (fig. 4).

Junkers follows the practice of stiffeners of closed channels, set fairly close together (fig. 5). The bulk-heads of high Z-sections are routed for the continuous stiffeners to which they are attached by half-round flange fittings. An example of a shell body with four reinforced stiffeners which extend forward into the four strong flanges of the center piece is represented in the Junkers body shown in figure 6. Here the Z-section bulkheads are interrupted to pass the four heavier stiffeners and at-

tached to the others by small angle fittings joined at the webs. A shell body built by Dornier is very similar. It has four continuous heavy longitudinal flanges of thick-walled T-section, while the remaining tubular stiffeners are interrupted at the bulkheads touching the skin (fig. 7). This body is contrary to orthodox practice, wider than it is high.

The Bayerische Flugzeugwerke have developed a particularly interesting type. The metal skin consists of separate panels bent on one end into a Z-section. These "bulkheads" are routed to permit passage of the U-channel stiffeners (fig. 8). These panels are first riveted together lengthwise and joined to the inserted stiffeners. Then the thus-obtained reinforced panels are joined together in the uppermost and lowermost part of the circumference to a wider stiffener which serves as butt covering.

In one Arado shell body the skin consists of longitudinal panels, every second one of which is bent at both ends into form-stiffener sections, in contradistinction to the Northrop method (reference 1), where each panel is angle-shaped at one end.

#### II. DETERMINATION OF STRESS CONDITION

### 1. System and Loading

In order to grasp the most essential characteristics of the stress condition of shell bodies - whether theoretically or experimentally - it first is necessary to simplify their system and loading.

The designed shell bodies have, in general, a length which is a multiple of the sectional dimensions (1/h = 6 to 9; in cross section they are usually of oval shape, widening out downward or upward, with a height slightly greater than the width. In many cases the section is elliptic, or even round, as in some U.S. shell bodies. The body shell may be largely considered as being cylindrical or conical, because the usual body form tapers from an almost cylindrical centerpiece very gradually toward the tip. For many fundamental studies the assumption of circular cylinder is sufficient.

On the basis of this outer form of the shell bodies,

it may be assumed that their stress condition on the whole is in agreement with the elementary "beam" theory, which postulates a great length compared to cross-sectional dimensions and a gradual change in cross-sectional form over the length. Another assumption of the elementary beam theory is that the sections under load undergo no substantial form change - that is, possess the necessary transverse stiffness, a condition likewise met by the shell body with sufficiently rigid and properly spaced bulkheads. After all, it should be borne in mind as regards shell bodies, even with still unbuckled skin, that by virtue of its greater circumferential extent and lower transverse stiffness than on the usual beam, the actual stress condition departs to a greater extent from that of an ideal beam computed according to Navier's flexure theory or St. Venant-Bredt's torsion theory. The disturbances are primarily due to the introduction of stresses not in accord with the beam theory and their directional changes at cutaway sections. Further disturbances are set up by the restrained warping of sections under transverse load flexure and twisting.

Other stress deflections are encountered on reinforced shell bodies with skin which is not buckling-resistant up to the failing load once the panels between the stiffeners have buckled under compression and shear.

The stress in the shell body is the result of the air loads on the wings and tail applied at the points of attachment; further, of the propeller loads transmitted by the engine mount and the ground forces due to landing gear or float system and tail skid. These are supplemented in the attachment points by the mass forces necessary for equilibrium of the structural parts attached to the body. Lastly, there are active mass forces distributed over the body length but whose effect, compared to the other forces, is small and which may be allowed for as forces combined in several points. It is thus primarily a case of concentrated loads which stress the shell body visualized as beam in bending and torsion. Bending of the end shell of the body is usually contingent upon a down load, and the torsion and lateral deflection on an eccentrically applied side load.

# 2. Stress Condition of Unstiffened Thin-Walled Shells

a) Elementary theory. - As basis of the subsequent arguments, we shall first investigate the stress condition of an unstiffened thin-walled cylindrical shell under flexure and twist. The wall thickness s may vary over the circumference, although it is assumed to be small with respect to the transverse dimensions of the shell. There are no stiffeners for the present but bulkhoads spaced sufficiently close are assumed to preserve the cross-sectional form.

The classical theory of beam flexure established for the beam of solid cross section results in linearly distributed tension stresses  $\sigma$  and derivated shear stresses  $\tau$ :

$$\sigma = \frac{B_z}{J_z} y + \frac{B_y}{J_y} z, \qquad \tau = \frac{Q_y}{J_z} \frac{S_z}{b_z} + \frac{Q_z}{J_y} \frac{S_y}{b_y}$$

whereby:

y, z are the respective distances of the relevant fibers from the principal axes of inertia.

$$J_z = \int_{F}^{x^2} dF$$
,  $J_y = \int_{F}^{x^2} dF$  the principal moment of inertia.

$$\underline{S}_z = \int y \ dF$$
,  $\underline{S}_y = \int z \ dF$  the static moments of the isolated cross-sectional piece with respect to the principal axes of inertia.

by, bz the section widths.

By, Bz the bending moments about axis y and axis z.

Qy, Qz the transverse loads in axis y- and axis z-direction.

In the application of the beam theory to thin-walled sections (fig. 9), it may be assumed that the tension and shear stresses are evenly distributed over the wall thickness s. Then the "shear flow" t = Ts, according to elementary theory of flexure is:

$$t = \frac{Q_y}{J_z} \underline{S}_z + \frac{Q_z}{J_y} \underline{S}_z = t_y + t_z$$

The inertia moments are:

$$J_z = \oint y^2 s du$$
,  $J_y = \oint z^2 s du$ 

and the static moments:

$$\underline{S}_{z} = \int_{0}^{u} y s du + \underline{S}_{z}(0)$$
 or  $\underline{S}_{y} = \int_{0}^{u} z s du + \underline{S}_{y}(0)$ 

Hereby u denotes the circumferential length measured from any zero point as far as the particular point. For closed symmetrical sections the choice of the points of symmetry as zero points is advisable, so that

$$\underline{\mathbf{S}}_{\mathbf{z}}(0)$$
 and  $\underline{\mathbf{S}}_{\mathbf{y}}(0) = 0$ 

otherwise, the constants  $\underline{S}_z(0)$  and  $\underline{S}_y(0)$  must be determined from the condition of torsion free bending:

$$\oint \frac{t_y}{sG} du \quad \text{or} \quad \oint \frac{t_z}{sG} du = 0$$

To insure torsion-free bending, the individual transverse loads must be applied at the "shear center," which for symmetrical sections lies on the axis of symmetry; for unsymmetrical sections its position must be defined from the condition that the shear flows  $t_y$  and  $t_z$  must possess no moment with respect to the shear center.

Transverse loads applied outside of the shear center can be represented by transverse loads in shear center and pure torsional moments  $M_{\rm X}$  on the longitudinal axis; they stress the cylinder in bending and torsion. In torsion, St. Venant's theory for solid sections affords, with unrestrained warping, a pure shear stress condition. For thinwalled closed sections a shear stress constant over the wall thickness may be assumed. Then, according to Bredt, the uniform shear flow for a twisting moment

$$T_{X} = \sum_{O}^{M} M_{X}$$

and the enclosed surface Fo is:

$$t_x = \frac{T_x}{2F_0}$$

and the torsional stiffness is:

$$G J_{T} = \frac{4F_{0}^{2}}{\int \frac{du}{sG}}$$

The results obtained for cylinders from the elementary theory of bending and torsion can be applied with the same degree of approximation to tapered shells. Then it must be observed that in bending the maximum tension stresses  $\sigma$  occur in sections perpendicular to the surface elements and have components in transverse load direction. The shear stresses  $\tau$  in these sections then have to carry only a share  $\overline{Q}$  of the transverse load Q. Then (fig. 10):

$$\sigma = \frac{B y}{J \cos \alpha}, \quad t = \tau s = \frac{\overline{QS}}{J}$$

with

$$\overline{Q} = -P_0 \frac{x_0}{x} - P_1 \frac{x_1}{x} - \dots$$

$$B = -P_0 (x - x_0) - P_1 (x - x_1) - \dots = (Q - \overline{Q}) x$$

Here J and S denote the respective inertial and static moment, computed with the smallest wall thickness s (in direction of the normals of the shell surface),  $\alpha$  is the angle of the surface elements to the longitudinal axis, x,  $x_0$ ,  $x_1$ , ... the respective distances of the section or load points from the cone tip of the relevant section point.\*

b) Membrane shell theory. - Substitution of the membrane shell theory for the elementary beam theory affords

<sup>\*</sup>Instead of distances from cone tip the heights at the sectional or loading point can be introduced. See Wagner: Luftfahrtforschung, vol. 13, no. 9, 1936, pp. 281-292. This also contains a detailed study of the bulkhead stresses.

a more accurate picture of the actual stress condition in thin-walled transversely reinforced cylinders (reference 2). The membrane theory stipulates, as is known, vanishing flexural and torsional stiffness of shell surface, thus leaving only the "membrane stresses"  $\sigma_x$ ,  $\sigma_y$ T constant over the wall thickness. The introduction of the external forces in cylindrical and tapered shells with transverse stiffeners (bulkheads) is devoid of circumferential stresses ou according to the membrane theory. In pure - i.e., shear-free bending - of transversely reinforced cylinders, the linear distribution of the tensile stresses with the condition of sections remaining undistorted in its plane, is compatible with the membrane shell theory if the effect of the contraction in area is disregarded. Under pure torsion through torque at the end bulkheads, both theories give a pure shear stress condition if the sections remain unchanged across the length and left free to warp at the ends. In bending under transverse load and in torsion under torque on intermediate bulkheads themselves, the validity of the elementary beam theory is restricted to circular cylinders and circular cones of constant circumferential wall thickness. In shells of different section, restrained cross-sectional warping on the end bulkheads and loaded intermediate bulkheads, as well as points of abrupt sectional change, produce a disturbance in the elementary stress condition through self-stress conditions, which disappear quickly provided the bulkheads are rigid and closely spaced.

The above arguments are applicable for an introduction of a force conformably to elementary theory. Under other application of axial loads, shear loads and torque - in the latter two only with elastic bulkheads - such cumulative stresses, which disappear more or less according to bulkhead design, occur even on the circular cylinder. Goodey (reference 3) has treated the cumulative stresses for the special case of cylindrical shell of constant section clamped at one end to resist warping, and stressed at the other end under torque. He stipulated either rigid bulkheads in their plane at the ends alone or at infinitely close spacing. Wagner-Simon (reference 4) established a method for the determination of the cumulative stresses by the introduction of an axial load for the extreme case of the infinitely shear-resistant shell surface; again bulkheads spaced infinitely close together but of finite stiffness are assumed. The special case of the flat shell of rectangular section (box beam) had been treated earlier by Reissner (reference 5) for uniformly distributed torsion

load on the premises of infinitely close rigid partitions, and by the author, for any torsional load with elastic partitions of finite spacing (reference 6).

3. Stress Condition of Longitudinally Stiffened

Shells Prior to Buckling of Skin

a) Elementary theory .- A shell of wall thickness s with stiffeners of section F<sub>T</sub> and spacing b (fig. 11) can, by close stiffener spacing, be substituted by an unstiffened shell of mean wall thickness  $\rm s_m = \rm s + \rm F_L/b$ whose median surface passes through the common center of gravity of the stiffeners and the adjacent skin strip. The mean wall thickness sm serves for the determination of axial stresses, longitudinal stiffness, and shear flow, the skin thickness s for the shear stresses and the shear stiffness of the unstiffened shell. For shell stiffeners of corrugated sheet with wall thickness sw and length of corrugation bw, the mean wall thickness for the longitudinal direction is:  $s_m = s + s_w b_w/b$ . But of the entire shear flow, the corrugated sheet takes up the share tw =  $\frac{s_W b}{s b_W + s_W b}$  t, leaving the share  $t_H = \frac{s_v b_W}{s b_W + s_W b}$  t for the skin. As a result, the shear stiffness per unit length of the shell with corrugated sheet stiffeners increases to (s + sw b/bw) G, as against sG for the shell with individual stiffeners. Referring the shear stiffness to the mean wall thickness sm of the shell with corrugated sheet stiffeners, the reduced shear modulus:

$$G! = \frac{s + s_W b/b_W}{s + s_W b_W/b} G$$

must be introduced.

For wider spacing or different section  $F_{L,i}$  of the m stiffeners (fig. 11), it is more appropriate to compute the surface moment of the skin and stiffener section with respect to the principal inertia axes of the total section separately, whereby the inertia moments of the stiffeners themselves, may be ignored. Then the surface moments of the total section become:

$$J_z = \oint y^2 s du + \sum_{i=1}^{m} F_{L,i} y_{L,i}^2 (J_y correspondingly)$$

$$\underline{S}_{z} = \int_{0}^{u} y \, s \, du + \sum_{1}^{-1} F_{L,i} + \underline{S}_{z}^{(0)} \left(\underline{S}_{y} \text{ correspondingly}\right)$$

 $\underline{S}_z^{(0)}$  again follows as for the unstiffened shell from the condition of torsion-free bending and disappears if the zero point lies on an axis of symmetry.

With heavy stiffeners, the individual stiffeners with the attached covering strip in their common center of gravity can be visualized as being concentrated in m individual longitudinal flanges. These have the section:  $F_i = F_{L,i} + \frac{1}{2} \; (b_i \; s_i + b_{i+1} \; s_{i+1}). \quad \text{The forces in these}$  flanges are now concentrated axial forces, while the intermediate skin panels serve to take up the shear stresses only. In bending due to transverse loads as, say about axis z, the axial loads amount to:

$$L_{i} = \frac{B_{z}}{J_{z}} F_{i} y_{i} = \frac{F_{i} y_{i}}{m} B_{z}$$

and from

$$\frac{\partial L_{i}}{\partial x} = t_{i+1} - t_{i} = \frac{F_{i} y_{i}}{m} Q_{y}$$

$$\sum_{i} F_{i} y_{i}^{2}$$

The constant shear flow between the longitudinal flanges:

$$t_{i+1} = \frac{\sum_{i=1}^{\Sigma} F_{i} y_{i}}{\sum_{i=1}^{\infty} F_{i} y_{i}^{2}} Q_{y} + t_{1}$$

If the section is symmetrical to axis y, it affords:

$$t_1 = 0$$
 or  $t_1 = -t_m = \frac{1}{2} \frac{\partial L_m}{\partial x} = \frac{1}{2} \frac{F_m y_m}{\sum_{i} F_i y_i^2} Q_y$ 

according to whether the first shear penel or the mth

flange intersects the axis of symmetry (fig. 11).

In the absence of symmetry  $t_1$  must be defined conformably to the condition of torsion-free bending:  $\frac{m}{\sum_{i=1}^{m}\frac{t_i}{G_i}}=0.$ 

In pure torsion without restrained warping the shell with stiffeners has the same shear flow  $t_x=\frac{T_x}{2F_0}$  as the unstiffened shell; even the torsional stiffness is the same:

$$G J_{T} = \frac{4F_{o}^{2}}{\int \frac{du}{sG}}$$

In shells with corrugated sheet reinforcement the shear flow is distributed as described previously, over skin sheet and corrugated sheet; in the torsional stiffness the greater shear stiffness G (s +  $s_W$  b/ $b_W$ ) replaces Gs.

b) Statically indeterminate theory .- Just as the membrane-shell theory affords the departures in stress conditions from the elementary theory for the lengthwise unstiffened shell, so the same discrepancies for the stiffened shell can be analyzed by a statically indeterminate calculation of the simplified system with concentrated longitudinal flanges and pure shear panels (fig. 11). (Compare the report (reference 6) which treats the special case of "shell" with four longitudinal flanges and plane shear panels under torsion.) Having a shell with m longitudinal flanges and stiffened at the ends by (n - 1) intermediate bulkheads this system can be divided at the intermediate bulkheads into n cells joined together by m longitudinal anchorages each (fig. 12). Of these, three are statically necessary on each bulkhead; that is, the redundant anchorages (n - 1) make the system (m - 3) times statically indeterminate. Clamping the shell at one end adds another (m - 3) statically indeterminate.

The mathematical treatment is as follows: Select as statical indeterminate between each two cells (m - 3) groups of axial loads in themselves in equilibrium, such as the tensiom in each one of the redundant longitudinal anchorages and their counterforces in the three statically

necessary longitudinal anchorages, for example. Instead of these force groups  $X_1, X_2 \dots X_{m-3}$ , linear combinations of these can be introduced as statically indeterminate. (See fig. 12, for example.)

$$X_{a} = \alpha'_{1} X_{1} + \alpha_{2} X_{2} \dots + \alpha_{m-3} X_{m-3}$$
 $X_{b} = \beta_{1} X_{1} + \beta_{2} X_{2} \dots + \beta_{m-3} X_{m-3}$ 
 $X_{c} = Y_{1} X_{1} + Y_{2} X_{2} \dots + Y_{m-3} X_{m-3}$ 
etc.

But these groups of axial loads must not be linearly related; the requisite and sufficing condition is that the determinant of the factors  $\alpha$ ,  $\beta$ ,  $\gamma$  .... does not disappear.

Each axial load group X stresses only the two adjacent cells, producing axial loads diminishing linearly to zero in the longitudinal flanges and constant shear flow in the intermediate panels. These are supplemented by tensile stresses, bending moments, or plane stress conditions in the directly loaded, as well as in the two adjacent bulkheads, depending upon the design of the bulkheads as truss, frame, or solid wall. For the axial loads and shear flows due to the external loading, a possible equilibrium condition, such as that from elementary theory, for instance, is introduced. From the condition that in the final system the longitudinal displacements (warping) of consecutive cells must agree on every bulkhead, a system of linear elasticity equations:

$$\delta_{aa} X_a + \delta_{ab} X_b + \delta_{ac} X_c + \cdots \delta_{a,o} = 0$$

$$\delta_{ab} X_a + \delta_{bb} X_b + \delta_{bc} X_c + \cdots \delta_{b,o} = 0$$

$$\delta_{ac} X_a + \delta_{bc} X_b + \delta_{cc} X_c + \cdots \delta_{c,o} = 0, \text{ etc.}$$

is obtained for the statically indeterminate X.

The factors  $\delta_{ik}$  and  $\delta_{i,0}$  denote groups of longitudinal displacements of a statically determinate main system as a respective result of the axial load groups X = 1, or to the external load, and can be obtained from simple integrations or summations; the equations are solved by one of the known methods. The execution of the static-

ally indeterminate calculation for irregular systems with a large number of longitudinal flanges or bulkheads is tedious; but since stiffened shell bodies usually are symmetrical with respect to the normal or to the lateral axis, a proper choice of the statical indeterminates affords farereaching simplifications.

On stiffened shells of simple symmetrical section the (m - 3) statical indeterminates, occurring on each intermediate bulkhead or at the fixation, can be formed from  $\frac{m-2}{2}$  and  $\frac{m-4}{2}$  or from  $\frac{m-3}{2}$  each of symmetrical and antisymmetrical groups of axial loads, depending on whether the number of flanges is even or uneven. Likewise, the external load can be divided into symmetrical and antisymmetrical parts. The symmetrical and antisymmetrical load groups do not affect each other; i.e., the system of elasticity equations reduces to two unrelated partial systems having solutions only for the symmetrical or antisymmetrical load, respectively. Besides, the statically indeterminate axial-load groups can be so posed and arranged that consistently smaller zones contain groups of partial forces which of themselves are in equilibrium. Then the elastic influence range of the load groups themselves must become consistently smaller by rising order, according to the St. Venant principle. The statical indeterminates of higher order can therefore be disregarded. In the case of m = 6 of figure 12, for example, the third group Xc is of higher order, since four partial forces in the zone of half the circumference are already in equilibrium.

By cyclic symmetry of the system the axial-load groups can be formed so that the part loads of the individual axial-load groups act like the ordinates measured at the flanges of the sine and cosine lines over the circumference with 2, 3, 4, ... waves. This leaves only the conjugated symmetrical and antisymmetrical axial-load groups at the adjacent frames related to each other; and the equation system reduces to (m - 3) independent 3- or 5-term partial systems, according to whether the bulkheads in their plane are assumed to be rigid or elastic. Application of the external loads in the distribution conformable to elementary theory produces no statical indeterminate if the symmetry is cyclic. Application of these assumed loads in inverse direction, establishes their equilibrium with the actual external loads. Dividing these equilibrium groups in corresponding groups like the statically indeterminate axial-load groups, each will create only the conjugated statically indeterminate group of axial loads.\*

By finite number of flanges m, division of the equation system in (m - 3) unrelated partial systems is already insured by a finite number (<m - 8) of symmetry axes; for example, by m = 6 in figure 12, doubled symmetry is sufficient. Insufficient symmetry is usually accompanied by mutual interference due to the axial-load groups of higher order which, for the reasons cited above, may be neglected.

So, provided the systems of stiffened-shell bodies are not seriously unsymmetrical and the suggestion as to choice and arrangement of the statically indeterminate systems is followed, it suffices to set up and solve the circumferentially unrelated 3- and 5-term equation systems for the conjugated axial-load groups X. In addition, with increasing order the calculation can be restricted to consistently smaller longitudinal zones and finally omitted altogether. For equal or similarly dimensioned cells, the 3- and 5-term systems of equations represent differential equations of the second and fourth order with constant factors from which closed solutions are obtained for the statical indeterminates. And the solutions can be further simplified by the frequently permissible assumption of very many cells or infinitely close-spaced bulkheads, where the difference equations become the relevant differential equations.

4. Critical Stress Condition of Stiffened and

### Unstiffened Shells

a) Bending (compression) of unstiffened cylinder. When stressing a thin-walled cylinder in bending or eccentric compression the shell usually fails under a certain "critical" stress condition through secondary or local bulging in the compression zone. This local bulging hinges chiefly on the amount of compressive stress and curvature

<sup>\*</sup>This method corresponds to that suggested by Southwell for the calculation of cyclic symmetrical-space frameworks, in which the joint displacements are built up from characteristic solutions of the correlated partial-difference equation and the given external loads or displacements are decomposed in these characteristic solutions. (See R. & M. No. 1573, British A.R.C., 1935.)

existing at that point; the stresses and curvatures in more distant zones are not as effective. It is therefore very natural to assess the stability of any cylinder in bending from the stability of a circular cylinder in pure axial compression, wherein the uniform compressive stress and curvature of this circular cylinder corresponds to the bending-compression stress and curvature of the relevant cylinder at the most unfavorable spot; for variable radius of curvature r and variable compressive stress  $\sigma$  this is determined from the condition  $\sigma$  r = max. This method leaves one, in any case, on the safe side. According to various calculations for circular cylinders by Flügge (reference 7), the critical compressive stress in pure bending may exceed that in pure compression by 30 percent.

A circular cylinder stressed under pure axial compression is theoretically at its limit of stability if the compressive stress in the elastic range reaches the critical value:

$$\sigma_{k} = \frac{E}{\sqrt{3(1-v^2)}} \frac{s}{r} \approx 0.6 E \frac{s}{r} \text{ (for } v = 0.3)$$

This value unrelated to shell length retains its validity only so long as several longitudinal waves can form. For very short cylinders of length

$$l \le \pi \sqrt{\frac{r^2 s^2}{12 (1 - v^2)}} = 1.72 \sqrt{r s}$$

ir is:

$$\sigma_{k} = \frac{E \pi^{2}}{12 (1 - v^{2})} \left(\frac{s}{l}\right)^{2}$$

that is, the Euler stress for a strip of length 1. In very long cylinders (pipes) the Euler stress

$$\sigma_{k} = \frac{\mathbb{E} \pi^{2}}{2} \left(\frac{r}{l}\right)^{2}$$

causes a sidewise bulging of the entire shell. When the critical stresses lie in the superelastic range, E is replaced by a reduced modulus (reference 8).

That the theoretical value of the bulging stress

 $\sigma_k$  = 0.6 E  $\frac{s}{r}$  is never reached, has been proved in a multitude of experiments; the latter disclose figures from 30 to 60 percent lower. These discrepancies are mainly attributable to the unavoidable divergence of the thinwalled shell from its exact geometrical form. The effect of such preliminary bulging has been investigated by Donnell (reference 9). On the assumption that the failure of the shell wall stressed in compression and bending is contingent upon reaching the yield point  $\sigma_s$ , he arrived at the critical stress of

$$\sigma_{k} = 0.6 \text{ E} \frac{\text{s}}{\text{r}} \frac{1 - 1.7 \times 10^{-7} \left(\frac{\text{r}}{\text{s}}\right)^{2}}{1 + 0.004 \frac{\text{E}}{\sigma_{s}}}$$

or

$$\sigma_{k} = 0.3 \, \mathbb{E} \, \frac{s}{r} \left[ 1 - 1.7 \times 10^{-7} \left( \frac{r}{s} \right)^{2} \right]$$

for duralumin with E = 7,000 to 7,500 kg/mm<sup>2</sup> and  $\sigma_s$  = 28 to 30 kg/mm<sup>2</sup>.

The values computed by this formula are in good agreement with experimental values throughout the range of  $\frac{\mathbf{r}}{\mathbf{s}} = 300$  to 1,500.

b) Bending (compression) of stiffened cylinder. In a cylindrical shell consisting of stiffeners and bulkheads stressed in bending, the curved panels in the compressive zone between the stiffeners may bulge. And to these "partial shells" or "panels" the same assumption of uniform compressive stress and curvature between the stiffeners is applicable. For the case of freely rotatory supported edges and an arc length of the panel of

$$b \ge 2\pi \sqrt[4]{\frac{r^2 s^2}{12 (1 - v^2)}} = 3.44 \sqrt{r s}$$

Timoshenko (reference 10) obtained the critical compressive stress of

$$\sigma_{k} = \frac{E}{\sqrt{3(1-v^2)}} \frac{s}{r}$$

that is, the same value as for the full shell which, hereafter, is designated with  $\sigma_{\text{R}}.$ 

For smaller arc lengths, it is:

$$\sigma_{k} = \frac{E \pi^{2}}{3 (1 - v^{2})} \left(\frac{s}{b}\right)^{2} + \frac{E}{4\pi^{2}} \left(\frac{b}{r}\right)^{2}$$

The first summand denotes the buckling stress  $\sigma_P$  of the flat plate of width  $\,b\,$  linked at the edges; the second summand can be expressed with  $\sigma_P$  and the value  $\sigma_R$  related to the curvature radius. Then the critical compressive stress of the curved panel assumes the form of

$$\sigma_{k} = \sigma_{p} + \frac{\sigma_{R}^{2}}{4\sigma_{p}}$$
 for  $\sigma_{R} \le 2\sigma_{p}$ 

or

$$\sigma_{k} = \sigma_{R}$$
 "  $\sigma_{R} \ge 2\sigma_{P}$ 

Evolved on somewhat different limiting conditions, Redshaw (reference 11) derived the critical compressive stress as:

$$\sigma_{k} = \sqrt{\sigma_{R}^{2} + \left(\frac{\sigma_{P}}{2}\right)^{2} + \frac{\sigma_{P}}{2}}$$

For the respective limiting cases of full shell and flat plate, both formulas give the same limiting values  $\sigma_R$  and  $\sigma_P$ . In the entire intermediate range, Timoshenko's values are smaller than those of Redshaw; the greatest difference at  $\sigma_R \approx 2\sigma_P$  amounts to about 20 percent. For a partial shell or panel with rigidly clamped sides the actual values of the critical compressive stress probably lie between the two values. For rigid or elastically clamped edges the buckling stress of the relevant plate substitutes for  $\sigma_P$ . The effect of preliminary bulging can be allowed for in both formulas by expressing  $\sigma_R$  with a value of  $\sigma_R = 0.2$  to 0.4 E  $\frac{S}{r}$  diminished according to the ratio r/s instead of with the full theoretical value.

Before the curved panels of a stiffened shell bulge between the stiffeners, the shell itself may buckle as a whole or over a large portion as, for example, between two stiff bulkheads (fig. 13). Just as in the stress analysis

the longitudinal stiffness of the stiffeners was uniformly graded over the circumference, so the stability investigation can be effected on the basis of bending and torsional stiffness of the stiffener and bulkhead sections uniformly distributed over the circumference and the length. Owing to the unlike stiffness of the shell surface in longitudinal and transverse direction, it then constitutes a case of orthogonally antsotropic cylinder or panel. And the stability of the orthotropic cylinder itself in bending can be ascertained from the stability of a corresponding circular cylinder under pure axial compression. Von Dschou (reference 12) has treated this case on the basis of Flügge's buckling determinant. Neglecting the torsional stiffness, he respectively obtained - for the full cylinder and a curved sheet of sufficient length and width to allow several bulges circumferentially and longitudinally as smallest possible critical compressive stress:

$$\sigma_{k} = \frac{2 E}{r s_{x}} \sqrt{\frac{J_{x} J_{u}}{\frac{J_{x}}{s_{x}} + \frac{J_{u}}{s_{u}} \frac{s_{x}}{s}}}$$

Hereby  $s_x$  and  $s_u$  and  $EJ_x$  and  $EJ_u$ , respectively, are the sections distributed over the circumference and the length, and the bending stiffnesses per unit length. For the respective special cases of stiffeners alone or of bulkheads alone, it is:

$$\sigma_{k} = \frac{E}{\sqrt{3(1-v^2)}} \frac{s}{r} \sqrt{\frac{s}{s_{x}}} = \sigma_{R} \sqrt{\frac{s}{s_{x}}}$$

and

$$\sigma_{k} = \frac{E}{\sqrt{3(1-v^2)}} \frac{s}{r} \sqrt{\frac{s_{u}}{s}} = \sigma_{R} \sqrt{\frac{s_{u}}{s}}$$

with  $\sigma_R$  again as the critical compressive stress of the unstiffened cylinder.

On short shells several bulges may form but only circumferentially. For a short shell, only longitudinally stiffened (fig. 13) as, for example, in the compression zone of a stiffened shell body between two bulkheads, it is:

$$\sigma_{\rm k} = \sigma_{\rm E} + \sigma_{\rm R} \sqrt{s/s_{\rm x}}$$

Here  $\sigma_E = \frac{E \pi^2 J_X}{s_X l}$  is the Euler stress of the stiffened strip of length l. For a short shell with bulkheads only, it is:

$$\sigma_{k} = \sigma_{E} + \frac{\sigma_{R}^{2}}{\sigma_{E}} \frac{s_{u}}{s}$$

where  $\sigma_{\rm E} = \frac{{\rm E} \; \pi^2}{12 \; (1 - v^2)} \left(\frac{\rm s}{\it l}\right)^2$  is the Euler stress of the unstiffened strip of length  $\it l$ . For a long but narrow shell of width  $\it b$  stiffened longitudinally or transversely, in which only several longitudinal bulges occur, and if the longitudinal walls are pin-jointed, it gives:

$$\sigma_{k} = \sqrt{\sigma_{R}^{2} \frac{s}{s_{x}} + \sigma_{e}^{2}} \quad \text{or} = \sqrt{\sigma_{R}^{2} \frac{s_{u}}{s} + \sigma_{e}^{2}}$$

Herein

$$\sigma_{\rm e} = \frac{2\pi^2}{s_{\rm x}} \frac{E}{b^2} \sqrt{J_{\rm x} J_{\rm u}}$$

is the critical compressive stress of the equally stiff-ened flat plate with disregarded torsional stiffness.

From the above formulas by Dschou, it follows that a stiffened shell of proper length and width is not substantially more resistant to buckling than an unstiffened shell unless it is stiffened in both directions. If the stiffened shell is short, longitudinal stiffeners by themselves give the shell substantially more resistance to buckling, while bulkheads alone avail little. A shell must be long and narrow to insure the same increase in buckling stiffeness with bulkheads as with stiffeners. The validity of the quoted buckling stresses  $\sigma_{\bf k}$  is, however, predicated on the absence of local bulges in the reinforcements and panels. Appearance of the stress  $\sigma_{\bf R}$  in the formula makes the inclusion of the preliminary bulging effect necessary.

An entirely different kind of stability failure may occur in a long, not unduly thin-walled cylinder without bulkheads when in bending the sections flatten out and the entire shell finally collapses. This case has been studied for the first time by Brazier, as applied to the iso-

tropic circular cylinder, and subsequently, by Heck (reference 13) to the orthogonally anisotropic elliptic shell. The critical stress of the longitudinally stiffened shell in the extreme fiber is, according to Heck:

$$\sigma_{k} = k \frac{E}{\sqrt{(1 - v^{2})}} \frac{s}{r} \sqrt{\frac{s}{s_{m}}}$$

in the elastic range.

k is approximately equal to 0.3 for the circular cylinder and also for slightly elliptic cylinders. The formula resembles Dschou's buckling formula for the stiff-ened circular cylinder, with the exception of the numerical factor, which is only about half as great. With the necessary reduction of the previously obtained theoretical values as a result of the preliminary bulging effect, the value from the last theory is in good agreement with test data. Usually, however, the failure is a local stability failure rather than a collapse because of the generally employed bulkheads.

c) Torsion (shear) and combined stress (compression and shear). - The critical shear stress of an unstiffened circular cylinder in torsion can be expressed by Donell's (literature quoted in reference 14), which for thin-walled

shells of finite length  $\left(\frac{1}{r} < 6.5 \sqrt{\frac{r}{s}}\right)$  with v = 0.3 and freely supported edges, gives:

$$\tau_{k} = 0.815 \ \mathbb{E} \left(\frac{r}{l}\right)^{1/2} \left(\frac{s}{r}\right)^{5/4}$$

For very long cylinders (pipes) with v = 0.3, it is:

$$\tau_{\rm k} = 0.29 \, \mathbb{E} \left( \frac{\rm s}{\rm r} \right)^{3/2}$$

Schwerin's formula for the critical twisting stress of infinitely long circular cylinders is similar, but his numerical factor is only 0.25. The theoretical values  $\tau_k$  must again be reduced 60 to 80 percent to allow for the preliminary bulging effect.

Shorter, unstiffened circular cylinders  $\left(\frac{l}{r} < 5\right)$  may

be treated by Ballerstedt and Wagner's formula (reference 15):

$$T_k = 0.1 E \frac{s}{r} + k E \left(\frac{s}{l}\right)^2$$

For freely supported sides use k=5.0; for clamped sides, k=9.1. For vanishing curvature, the formulas give approximately the critical shear stress of the freely supported and clamped flat strip of infinite length (k=4.85 and k=8.15, respectively). The formula was confirmed by Ballerstedt and Wagner on circular cylinders of  $\frac{r}{s}=250$  to 4.000, and  $\frac{1}{r}=0.25$  to 2.0 as well as by Lundquist's experiments (reference 16), in the range of  $\frac{r}{s}=340$  to 1.400 and  $\frac{1}{r}=0.2$  to 5.0.

The panels of width b in a stiffened cylinder can again bulge between the stiffeners under twisting stress. This case has not been theoretically explored heretofore, although Timoshenko's or Redshaw's formulas for the curved panel under compression may be employed for the critical shear stresses:

$$\tau_{k} = \tau_{P} + \frac{\tau_{R}^{2}}{4\tau_{P}}$$
 for  $\tau_{R} \le 2\tau_{P}$ 

$$\tau_{k} = \tau_{R}$$
 for  $\tau_{R} \ge 2\tau$ 

 $\tau_{k} = \sqrt{\tau_{R}^{2} + \left(\frac{\tau_{p}}{2}\right)^{2} + \frac{\tau_{p}}{2}}$ 

and

Herein T<sub>R</sub> is the buckling stress of the unstiffened full shell, according to one of the cited formulas and T<sub>P</sub> = 4.85 and 8.15 E  $\left(\frac{S}{b}\right)^2$ , respectively; the critical shear stress for the freely supported and the clamped strip. The thus-computed critical shear stresses are in satisfactory agreement with experimental data. The dimensions of the three circular cylinders in the DVL tests were:  $\frac{r}{s}$  = 600, 800, 1,000;  $\frac{b}{s}$  = 150, 400, 350;  $\frac{1}{r}$  ≈ 5.0. Timoshenko's values were on an average 10 percent lower, and Redshaw's figures about 10 percent higher than the experimental values. The buckling stress T<sub>R</sub> was expressed by Ballerstedt and Wagner's value.

Under bending with transverse load as well as combined bending and torsion, the panels manifest axial stresses due to bending superposed by shear stresses due to transverse load and torsion (fig. 13). The relevant critical compressive and shearing stresses  $\sigma_k$  and  $\tau_k$  which induce failware if concurrent, may be determined from

$$\left(\frac{\tau_{k}}{\tau_{k,o}}\right)^{n} = 1 \rightarrow \frac{\sigma_{k}}{\sigma_{k,o}}$$

where  $\sigma_{k,o}$  and  $\tau_{k,o}$  signify the critical stress in pure compression and pure shear, respectively. The exponent n is n = 2, according to Ballerstedt and Wagner, and n  $\approx$  3, according to U.S. experiments (reference 16). Under superposed tensile and shearing stresses it is, according to Ballerstedt-Wagner (reference 17):

$$\frac{\tau_{k}}{\tau_{k,0}} = 1 + \frac{1}{2} \frac{\sigma_{k}}{\sigma_{k,0}}$$

5. Stress Condition of Stiffened Shells

after Bulging of Skin

a) Flat panel in compression .- Bulging of the panels between the stiffeners as a result of compression or shear load does not, however, exhaust the load capacity of the stiffened shell under bending or torsion. The stiffeners, and to a certain extent the buckled panels themselves, remain capable of supporting additional compressive loads; likewise, the panels, acting as diagonal tension fields can, in conjunction with the stiffeners, transmit further shear loads. Permanent deformations of the bulged panels after abatement of the load, is usually not to be feared in the thin-walled metal designs of aircraft, because the panels usually bulge far below the elastic limit and would require more substantial bending stresses before that limit is exceeded. This explains the importance attaching to the stress condition of shell bodies after bulging of the metal skin.

Take the simplest case of flat panel under pure compression after bulging; the sides of the panel bounded by the stiffeners are to remain straight under the load. Further compression of such a sheet after bulging causes

the mean longitudinal fibers to deflect more than the outer fibers, and so avoid any subsequent stress absorption because their contraction does not follow as elastic crushing but as geometrical contraction of the chord with respect to the arc. So, under increasing load, the compressive stress in the center remains almost the same as at bulging, while manifesting a marked rise toward the sides (fig. 14). The same holds true in transverse direction of the sheet. Owing to this, the sides would give inwardly in the middle if the stiffeners or the adjacent sheet panels did not prevent that. This constraint produces stresses in transverse direction which with nonshifting sides form a resultant transverse tension. The thus created stress condition was deduced by Marguerre and Trefftz (reference 18) from the theory of plates with "great" deflection on the basis of the bulge form shortly after bulging. Marguerre (reference 19) then extended the study to bulge forms encountered in shell bodies after considerably exceeded buckling load.

For the practical calculation, the concept of "apparent" or "effective" width is very expedient. Visualize at the edge, stiffeners fully supporting sheet strips of such width that they carry the same load as the whole sheet panel. With  $\sigma_L$  = stress in edge stiffeners, and  $\sigma_m$  = mean stress of the whole sheet panel of width b, the apparent width is defined by (fig. 14):

$$b_{m} \sigma_{L} = b \sigma_{m} = \int_{-b/2}^{+b/2} \sigma_{x} dy$$

An estimate of the apparent width which lies on the safe side can be obtained, according to von Kármán, in the following manner: The load capacity of a plate of width b and thickness s is — if its buckling stress  $\sigma_k$  is considered as stress limit —

$$P = \sigma_k s b = k E \left(\frac{s}{b}\right)^2 s b = k E \frac{s^3}{b}$$

Herein k denotes a numerical factor depending on the edge support and the aspect ratio. Conformably to this formula, the plate carries so much more as its width is less. On the other hand, there is a limit to which the width may be reduced; that is, the buckling stress may not exceed the critical compressive stress  $\sigma_{\text{L}}$  of the edge

sections nor the yield point. Kármán then assumes that the plate, width b, stressed beyond its buckling limit, has at least the same load capacity as a narrower plate of width  $b_{\rm m}$ , whose buckling stress  $\sigma_{\rm k,m}$  is precisely equal to the limiting stress  $\sigma_{\rm L}$ :

$$\sigma_{k,n} = k E \left(\frac{s}{b_n}\right)^2 = \sigma_L$$

Therefrom follows the "apparent" width at

$$b_{m} = \sqrt{\frac{kE}{\sigma_{L}}} s = \sqrt{\frac{\sigma_{k}}{\sigma_{L}}} b$$

For the plate hinged at the sides, it is:

$$b_{\rm m} = 1.9 \sqrt{\frac{E}{\sigma_{\rm L}}} \text{ s}$$

and the mean stress becomes:

$$\sigma_{\rm m} = \frac{b_{\rm m}}{b} \sigma_{\rm L} = \sqrt{\sigma_{\rm k} \sigma_{\rm L}}$$

The formula for  $b_m$  or  $\sigma_m$  can equally well be employed to compute the stresses  $\sigma_L > \sigma_k$  in the stiffeners of section  $F_L$  by given compression load P. One may estimate  $\sigma_L$  first, and then check whether or not the stress

$$\sigma_{L} = \frac{P}{F_{L} + b_{m} s} = \frac{P - \sigma_{m} b s}{F_{L}}$$

defined with the values  $\,b_m\,$  or  $\,\sigma_m\,$  corresponds to the first assumption. If not, then the rapidly convergent process is repeated.

Evolved on a simplifying assumption for the stress condition ( $\sigma_y = \tau = 0$ ), which is, however, as treated in detail in Marguerre's report, precarious - especially, in view of the noncompliance of the sides to remain straight - Cox obtained as share of the apparent width:

$$\frac{b_{\rm m}}{b} = \alpha \sqrt{\frac{\sigma_{\rm k}}{\sigma_{\rm L}}} + \beta$$

His findings for freely supported sides are:  $\alpha=0.80$  and  $\beta=0.09$ , for clamped sides;  $\alpha=0.82$  and  $\beta=0.14$ . Adapting the coefficients to the more accurate results of Marguerre, it is better to put  $\alpha=0.81$  and  $\beta=0.19$  for freely supported sides which, even in the limiting case  $\sigma_{k}=\sigma_{L}$  gives the correct value  $b_{m}=b$ . Marguerre suggests a very simple approximate formula, which is in good agreement with the exact results:

$$\frac{b_{\rm m}}{b} = \sqrt{\frac{\sigma_{\rm k}}{\sigma_{\rm L}}}$$

Figure 15 is a comparison of the apparent widths versus  $\sigma_L/\sigma_k$ , according to various theories and formulas, including the experimental values obtained by Lahde and Wagner (reference 20). The curve, conformable to Marguerre's approximate formula, is in satisfactory accord with the test points, whereas the curve according to Kármán's formula, gives throughout, too small values. The theoretical curve according to Treffttz-Marguerre, and correspondingly, the curve according to Cox's improved formula, are in good agreement with the experiments so far as the buckling load is not too much exceeded; if exceeded very much, the values are too great. This is due to the fact that the buckling form serving as basis of the theory, does not resemble accurately enough the actual buckling form incurred under greatly exceeded buckling load.

b) Curved panel under compression. Theoretical investigations concerning the apparent width of curved panels buckled in compression are as yet lacking. Newell (reference 21) made some experiments with unstiffened curved sheets, whose sides were carried in V-shaped grooves which allowed tangential - but no radial - shifting of the sides in circumferential direction. But such an arrangement carries little resemblance to the actual conditions of a curved panel between two stiffeners of a shell body.

An estimate of the load capacity and of the apparent width of a curved panel can be obtained as follows: If the sheet is curved, the curvature itself affords an additional load capacity which is not dependent on the stiffener spacing. The load that a sheet can carry because of its curvature, is:

$$P_R = \sigma_R$$
 b s, with  $\sigma_R \approx 0.3 E \frac{s}{r}$ 

Then the portion between the stiffeners supported as "plate" needs to carry only the difference between the total panel load and the curvature share  $P_R$ . Then as edge stress of this plate the difference  $(\sigma_L - \sigma_R)$  is in force rather than the stiffener stress  $\sigma_L$ . The apparent width of the curved sheet is expressed with  $\overline{b}_m$  to differentiate it from that of the flat sheet  $b_m$  and the difference  $(\sigma_L - \sigma_R)$  substitutes for  $\sigma_L$  and the buckling stress  $\sigma_P$  of the flat plate of width b for  $\sigma_L$ . Then the load capacity of the sheet by virtue of its plate effect becomes:

$$P_P = (\sigma_L - \sigma_R) s \overline{b}_m$$

and the total load capacity of the curved panel is:

$$P_R + P_P = \sigma_R s b + (\sigma_L - \sigma_R) s \overline{b}_m = \sigma_L s b_m$$

Therefrom follows the apparent width of the curved sheet at

$$b_{\rm m} = \overline{b}_{\rm m} + \frac{\sigma_{\rm R}}{\sigma_{\rm L}} (b - \overline{b}_{\rm m})$$

wherein, if the apparent width of the flat sheet freely supported at the sides is computed, say, according to Marguerre, we must introduce:

$$\overline{b}_{m} = \sqrt[3]{\frac{\sigma_{p}}{\sigma_{L} - \sigma_{R}}}$$
 b with  $\sigma_{p} = 3.6$  E  $\left(\frac{s}{b}\right)^{2}$ 

The validity of the formula for  $b_m$  was checked by the DVL in a series of tests on reinforced panels (fig. 16) divided by stiffeners, into several (3 to 5) curved sheets, the two ends being bolted to angle sections as shown in the figure. The panels were compressed between parallel plates in a 20-ton hydraulic press. The tests were made with curved sheets of different curvature and thickness (r/s = 500, 800, 1,000, 2,000,  $\infty$ ) and different stiffener sections. The dimensions of the individual panels may be seen in figures 17 and 18.

The test stations at which the measurements were made and the mean compressive stress values  $\sigma_L$  computed, are shown in figures 17 and 18. Based upon these measurements,

the apparent width was then obtained in the following manner: The total load capacity of the stiffeners with total section  $\Sigma F_L$  is:  $P_L = \sigma_L$   $\Sigma F_L$ . The difference between the total applied load P and the load capacity  $P_L$  then represents the load of the n skin panels alone:  $P_H = P - P_L = n$  s  $b_m$   $\sigma_L$ , from which the apparent width at each stiffener then follows at:

$$b_{m} = \frac{P - \sigma_{L} \Sigma F_{L}}{n s \sigma_{L}}$$

Figures 17 and 18 give the experimental apparent widths versus mean profile stress. The curves of the apparent width of the curved sheet as derived from the previous formula, are also shown by comparison. The apparent width bm of the panels with open channel stiffeners was computed with

$$\overline{b}_{\text{m}} = 1.63 \sqrt{\frac{E}{\sigma_{\text{L}} - \sigma_{\text{R}}}} \text{ s + 0.14 b}$$

and for those with closed stiffeners corresponding to the stronger fixity of the panels, with

$$\bar{b}_{\rm m} = 2.15 \sqrt{\frac{E}{\sigma_{\rm L} - \sigma_{\rm R}}} \, s + 0.14 \, (b - e)$$

Herein b denotes the spacing of the profiles\_and e the spacing of the two rivet rows. The computed  $b_m$  is counted outward from the rivet rows. In panels with closed channel stiffeners the sheet between the rivet rows is figured as being fully supporting. The curvature stress was written in at  $\sigma_R = 0.3 \ E \frac{s}{r}$ ; the elastic modulus at  $E = 740,000 \ kg/cm^2$  for duralumin.

The comparison of the test values with those from the proposed formula discloses for the greatly curved sheets (r = 200 mm) a good agreement at the beginning; while for the shallow curvature of shells with open sections, the computed values are slightly higher than the experimental values; in shells with closed sections it is the opposite, probably owing to the better support of the sheet panels with the closed sections. Every experimental curve of the shell of 0.4 mm thickness, reveals in the vicinity of

 $\sigma_L = 1,000 \text{ kg/cm}^2$  — on the open sections a little before, on the closed one a little behind — a distinct break. This is the point where the buckling stress of the sheet between the rivets spaced at t=20 mm is reached. For full fixation, this amounts to

$$\sigma_{\rm k} = \frac{\pi^2}{3} \frac{E}{1 - v^2} \left(\frac{s}{t}\right)^2 = 1,070 \text{ kg/cm}^2$$

From here on there is no substantial increase in load capacity of the skin  $P_H=\sigma_L$   $b_m$  s; that is, the apparent widths plotted against  $\sigma_L$  resemble equilateral hyperbolas. The panel of 0.5 mm thickness, reveals no break at  $\sigma_L=1,000~kg/cm^2$ , but evinces at  $\sigma_L=1,500~kg/cm^2$  (i.e., buckling stress of sheet of 0.5 mm thickness) a marked departure from the theoretical curve.

Summed up, the given formula for assessing the apparent width in shells of curved sheet is practical so long as the sheet is not buckled between the rivets; for shells with open sections the values being a little too high, for those with closed sections a little too low. In this range the apparent width is substantially enhanced by the curvature, as seen on comparison with the flat sheet curves of figures 17 and 18. Following the buckling of the sheet between the rivets, however, the apparent width of the curved sheet diminishes much faster than the theoretical curves indicate, and drops in proximity of the failing condition to approximately the value of the flat sheet (fig. 40). Further data on the effect of rivet spacing in its relation to the load capacity of stiffened shells will be found in an article by Kromm (reference 22).

c) Stiffened full shell with buckled panels under pure bending. On knowing the stress condition of the curved panel buckled in compression, the stress condition of the stiffened full shell with panels buckled in pure bending can then be ascertained. We first determine the rectilinear stress condition  $\sigma_0$  on the assumption of fully supporting skin in the compression zone; then ascertain with one of the formulas cited in section 4a, which panels in the compression zone buckle, and then compute on the stiffeners the apparent widths  $b_{m,1}$  of the buckled panels from one of the previously cited formulas by introducing the stresses  $\sigma_{L,0}$  for fully supporting skin in the first calculation process. The result is a new cross

section only partially supporting in the compression zone, from whose inertia moment referred to the new zero line

$$J_1 = \sum (F_L + b_{m,1} s)_i y_i^2$$

follows an improved straight stress condition  $\sigma_1$ . This then gives more exact values  $b_{m,2}$  and  $J_2$  for the apparent widths and the inertia moment from which a further improved stress condition  $\sigma_2$  can be obtained, etc. In general, however, the stresses  $\sigma_2$  themselves, diverge so little from  $\sigma_1$ , that one or, at the most two, calculation processes are sufficient. A simpler but somewhat less accurate method is to define the new stresses  $\sigma_{L,1}$   $\sigma_{L,2}$ , etc., directly from the stresses  $\sigma_{L,0}$  of the fully supporting cross section and the apparent widths  $b_{m,1}$ ,  $b_{m,2}$ , etc.:

$$\sigma_{L,1} = \frac{F_L + b s}{F_L + b_{m,1} s} \sigma_{L,0}, \quad \sigma_{L,2} = \frac{F_L + b s}{F_L + b_{m,2} s} \sigma_{L,0}$$
 etc.

It eliminates the tedious second determination of the zero line and of the inertia moment, although leaves the stress distribution in the compression zone no longer rectilinear.

To check the proposed calculation method, we made some stress measurements on different stiffened circular cylinders under pure bending. The loading arrangement is seen in figure 19. The ends of the cylinder are reinforced by heavy steel rings to prevent local overstresses under load applications. It is secured on one end to an iron frame while the load is applied at the other through a couple of horizontally acting forces. This horizontal couple is the counter effect of a vertical couple formed by the tension of a hand winch and its counterforce on a lengthwise sliding roller bearing. The cylinder in figure 19 is of 0.4 mm wall thickness and 400 mm curvature radius and reinforced by 18 Z-section stiffeners (fig. 20). The ring frames, also of Z-sections, are spaced 360 mm apart and attached to the inside edge of the stiffeners. The stresses were measured in a mean section on every stiffener at three stations each (fig. 20) at loads up to 3/4 failing load. The mean values of these stresses for three different load increments are plotted against the stiffeners in

figure 20. The stress distribution, according to the elementary beam theory for all load increments and assumedly fully supporting skin, was also included for comparison. Comparison of the theoretical and experimental results disclose that under slightly exceeded buckling stress of the skin - the first skin buckles appeared at around 630 mkg bending moment - the real stress condition is still fairly obtained by the elementary beam theory if a fully supporting skin is assumed, while at the higher load stages the compression zone manifests appreciable differences. But with the more accurate method of the apparent width, the values for the highest load increment are in good agreement with the experimental values. The simpler method of maintaining the zero line of the fully supporting cross section gives, at the extreme compression fiber stresses, about 12 percent too high compared to the experimental values.

d) Reinforced full shell in bending with transverse load and torsion .- Bending with transverse load induces, apart from the buckles in the compression zone, oblique wrinkles due to the buckling of the panels as a result of shear, which begin in the neutral zone and, under further load increase, continue chiefly in the less shear-resistant compression zone (fig. 21). The formation of the oblique wrinkles creates a stress rearrangement because now the panel transmits chiefly tensile stresses in the direction of the wrinkles and the compressive stresses must be taken up by the stiffeners. Under greatly exceeded buckling stress the stress condition due to shear can be determined according to Wagner's tension bay theory (reference 23). Assuming a homogeneous distortion bay, the wrinkling angle a to the longitudinal direction is for the curved panel obtained from (reference 24):

$$\tan^2 \alpha = \frac{\epsilon_1 - \epsilon_x}{\epsilon_1 - \epsilon_y} = \frac{\sigma_1 - \sigma_x}{\sigma_1 - \sigma_y - E \zeta}$$

whereby  $\epsilon_1$  and  $\sigma_1$  are the principal elongation and principal stress, respectively, in direction of the wrinkles;  $\epsilon_{\rm x}$  and  $\epsilon_{\rm y}$  and  $\sigma_{\rm x}$  and  $\sigma_{\rm y}$ , respectively, the elongations and stresses of the side stiffeners in longitudinal and transverse direction. The value  $\xi$  is obtained for the curved sheet as a result of the fact that under increasing shear load the oblique skin wrinkles between the stiffeners are gradually pulled smooth. The sheet of

arc length b curved about the x-axis corresponds, after smoothing, to a flat sheet of height b, which prior to shear loading had been contracted through wrinkling in transverse direction for the difference between arc and chord. In the circular cylinder the "wrinkling" is approximately (reference 24):

$$\zeta = -\frac{1}{24} \left(\frac{b}{r}\right)^2$$

The principal stress in the tension bay becomes:

$$\sigma_1 = \frac{\tau}{\sin \alpha \cos \alpha} + \sigma_2$$

the normal stress in longitudinal direction:

$$c_n = \tau \cot \alpha + \sigma_2$$

and the normal stress in circumferential direction,

$$\sigma_{u} = \tau \tan \alpha + \sigma_{a}$$

The stress condition is first ascertained with an estimated value of the wrinkling angle and then progressively improved by insertion of the value found in the preceding step. The still undetermined principal stress og transverse to the direction of the wrinkles must be allowed for by an assumption (reference 25). The simplest way is to disregard og altogether as on the flat-plate beam. But this simplification as applied to the curved panel is less favorable on account of the generally less exceeded buckling load than for the flat panel. However, in place of  $\sigma_2 = 0$ , the principal stress  $\sigma_2$  during the subsequent load increase may be assumed as regards magnitude constantly equal to its value og,k at the instant of buckling or, when computing the stress condition in the tension bay, simply consider the excess of the load beyond the critical on buckling; i.e., for instance, under pure shear bending, utilize only the difference (T - Tr).

As proved by experiments the formation of a complete tension bay after buckling is no sudden process, but rather a gradual change from pure shear into pure tension bay (reference 26). As a result, the stiffener and bulkhead stresses attain to their full value only after the buckling

load has been substantially exceeded. This zone of transition of the "incomplete tension bay" is of particular importance for the stiffened shell with shear loaded curved panels, as in most cases failure occurs before the tension bays are completely formed. Besides, the shear stiffness of the panels in the transition zone is necessary for computing the strain condition of the shell. Schapitz treats the stress condition of an incomplete tension bay under shear and compression (reference 27).

The transverse load in the stiffeners of a cylinder (fig. 11) produces additional compression loads due to the longitudinal stresses  $\sigma_n$  of the complete tension bays:

$$\Delta L_{i} = \frac{1}{2} (b_{i} s_{i} \sigma_{n,i} + b_{i+1} s_{i+1} \sigma_{n,i+1})$$

These additional compression loads are further supplemented as a result of the tension bays through the deflection of the tension wrinkles at the stiffeners by inward radial loads  $\mathbf{q_r}$  and under unequal stress or observation of adjacent bays by tangential loads  $\mathbf{q_u}$ , which are defined through the circumferential stresses  $\sigma_{\mathbf{u}}$  of the tension bays. In the circular cylinder with stiffeners of not too great spacing b it is:

$$q_{r,i} = (\sigma_{u,i} + \sigma_{u,i+1}) \frac{sb}{2r}$$

$$q_{u,i} = (\sigma_{u,i} - \sigma_{u,i+1}) s$$

These additive loads strain the stiffeners in bending, and their support loads the bulkheads in bending and compression. The radial loads increase toward the neutral zone; for that reason if the shell is stressed in bending and transverse load, the compression-bending stress of the stiffeners nearer to the neutral zone may become more serious than the compressive stresses of the stiffeners in the extreme compression zone.

The stress distribution in bending with transverse load on the cylinder illustrated in figure 22, was established through various stress measurements. The loading was effected as a concentrated load applied at the stiffener ring of the free end. The stresses were measured on all stiffeners in three sections at the same load increment (fig. 22), and in a further section at three different

load stages as well as for a pure bending moment corresponding to the highest load stage (fig. 23). The diagrams give the averages of the measured stresses for three test stations each of the two symmetrical stiffeners and the computed values with and without allowance for the compression stresses created by the tension bays. These additive stresses were computed from the excess  $(\tau - \tau_k)$  on the assumption of a complete tension bay as follows: The normal force in the i<sup>th</sup> tension bay in longitudinal direction is

$$N_i = \sigma_{n,i}$$
 b s =  $(T_i - T_{k,i})$  cot  $\alpha_i$  b s

The critical shear stress  $\tau_{k,i}$  is expressed in every bay with the relevant value of the combined tensile and compressive stress (section II,4,c).

In the individual bays of the formulas for the wrinkling angles  $\alpha$ , the mean values of the stresses  $\sigma_{\rm X}$  and  $\sigma_{\rm y}$  of the opposite side members due to bending and additional stress through the tension bays, were introduced. For the bending stresses we assumed at the stiffeners the effective sheet strips resulting under pure bending, while for the additive stresses, only the strip between the two rivet rows of the hat section was added to the section of the stiffener. In the transverse elongation  $\epsilon_{\rm y}$  the compression of the bulkheads and the mean deflections of the stiffeners due to radial loading  $q_{\rm r}$  were also allowed for in addition to the wrinkling effect.

The tension loads N<sub>i</sub> of the panels are balanced by the compression loads of the stiffeners. By immediate balance of the unlike loads N<sub>i</sub> in the different bays in the adjacent stiffeners, the end sections would have to be able to warp, which the stiff end rings, however, prevent. For this reason the resultant normal force of the loads N<sub>i</sub> is evenly, and its moment with respect to the center of gravity of the stiffeners (without covering) rectilinearly, distributed over it. Then the additional stress of the ith longitudinal flange becomes (cf. section II,3,a):

$$\Delta \sigma_{\text{L,i}} = \frac{\stackrel{\text{m}}{\overset{\Sigma}{\Sigma}} N_{\text{i}}}{\stackrel{\text{m}}{\overset{\Sigma}{\Sigma}} N_{\text{i}}} + \frac{\stackrel{\text{m}}{\overset{\Sigma}{\Sigma}} N_{\text{i}}}{\stackrel{\text{o}_{\text{i}}}{\overset{\text{o}_{\text{i}}}{\Sigma}}} + \frac{\overset{\text{m}}{\Sigma}}{\overset{\text{m}}{\Sigma}} F_{\text{L,i}} \stackrel{\text{v}}{\overset{\text{o}_{\text{i}}}{\Sigma}} + \frac{\overset{\text{m}}{\Sigma}}{\overset{\text{m}}{\Sigma}} F_{\text{L,i}} \stackrel{\text{v}}{\overset{\text{o}_{\text{i}}}{\Sigma}} + \frac{\overset{\text{m}}{\Sigma}}{\overset{\text{m}}{\Sigma}} F_{\text{L,i}} \stackrel{\text{v}}{\overset{\text{o}_{\text{i}}}{\Sigma}} + \frac{\overset{\text{m}}{\Sigma}}{\overset{\text{m}}{\Sigma}} F_{\text{L,i}} \stackrel{\text{v}}{\overset{\text{o}_{\text{i}}}{\Sigma}} + \frac{\overset{\text{m}}{\Sigma}}{\overset{\text{m}}{\Sigma}} F_{\text{L,i}} \stackrel{\text{m}}{\overset{\text{m}}{\Sigma}} F_{\text{L,i}} \stackrel{\text{m}}{\overset{\text{m}}} F_{\text{L,i}} \stackrel{\text{m}}{\overset{\text{m}}{\Sigma}} F_{\text{L,i}} \stackrel{\text{m}}{\overset{\text{m}}{\Sigma}} \stackrel{\text{m}}{\overset{\text{m}}} F_{\text{L,i}} \stackrel{\text$$

with 
$$e_i = \frac{y_{L,i-1} + y_{L,i}}{2}$$

These stresses were superposed on those

$$\sigma_{L,i} = \frac{B_z}{m} y_i$$

$$\sum_{i=1}^{L} F_i y_i^2$$

due to bending moment alone, i.e., without tension bay effect.

The comparison of the stresses in figure 22 shows that the recorded stresses lie on the average between those computed with and without tension bays. In the extreme compression zone they approximately reach the value of the tension bay theory; in the extreme tension zone they come nearer to the value of the elementary beam theory. The section V at the point of load application, as well as section I at the point of fixity, manifested a distinct S motion, which is not quite so pronounced on the test values of the middle section. This is attributable to the supplementary stresses set up in the rigid end rings as a result of the restrained warping. The warping without the end rings, as a result of the transverse load, follows from the lessened shear stiffness of the tension bays in the neutral zone. (Cf. section II,2,b.)

The stresses (fig. 23) recorded in section II in bending with transverse load are in good agreement with the values of the elementary theory for the first load stage, which is slightly below the buckling load, but disclose a greater divergence in the compression zone as the load is increased, while the measurements under pure bending conform to the elementary calculation even in the highest load stage. On the other hand, the tension bay theory is well complied with by the test values in the compression zone under transverse load and bending. In the tension zone the test points again approach the computed stress condition without tension bay influence. In short, under bending with greater transverse load - apart from minor disturbances due to restrained warping - the stresses in the extreme tension fiber are accurately enough analyzed by the elementary bending theory and in the extreme compression fiber by the tension bay theory.

In pure torsion and simultaneous bending and torsion of a stiffened shell, the tension bays formed after buckling of the skin, are the same as in bending with transverse load. If the bays are of equal size all tension bays are alike in pure twist (fig. 24). So the same arguments hold for the tension bay stresses and the additional stiffener stresses as before. But, while - as proved by the experiments - in bending with transverse load which relates to an additional stiffener stress due to the tension bays, the complete tension bay suffices as basis of the calculation, this assumption creates under preponderant torsion stress in thicker shells and weaker stiffeners, greater differences between theory and test. In this case an accurate calculation, evolved on the incomplete tension bay, is necessary. A detailed study of the stress condition in torsion of stiffened shells after buckling of the tension bays and a comparison of experimental data with different theories, has been made by Schapitz (reference 28).

### III. DETERMINATION OF FAILING STRENGTH

## 1. Failing Strength in Bonding

a) Effect of skin on failing strength .- The load capacity of a shell with buckling-resistant sheet panels and stiffeners under flexure is determined from the buckling stresses ok of its compression zone as given in section II,4. In a shell with buckled sheet panels the real shell effect is lost, and it then becomes a system of stiffeners and bulkheads. If the bulkheads are of adequate stiffness, the load capacity becomes exhausted when the stiffeners fail. Consequently, the buckling strength of the stiffeners governs the failing bending moment of such a shell. Depending on length and section, the failing of the longitudinals may occur in various forms: as Euler members perpendicular to the skin (flexural buckling) if consisting of members with closed profile and great length or wall thickness; the buckling of members with open profile is associated with a simultaneous twisting (torsional buckling); if of short length or very thin walls, the closed as well as the open profiles manifest local buckling. Whereas these three buckling forms are still mathematically calculable if the profile is bare (no skin), the additive covering introduces influences on the buckling process which are difficult to analyze.

To begin with, the skin raises the stiffness of the section effective for the flexural buckling. The relevant apparent width  $b_m$ ' of the sheet is not identical with the apparent width  $b_m$ . but follows from the longitudinal stiffness of the strip at the instant of buckling (reference 29):

$$\mathbb{E} \ \mathbb{F}! = \frac{\partial \left( s \ b_{m} \ \sigma_{L} \right)}{\partial \epsilon} = \mathbb{E} \ s \ \left( b_{m} + \sigma_{L} \ \frac{\partial b_{m}}{\partial \sigma_{L}} \right) = \mathbb{E} \ s \ b_{m}!$$

Since  $\frac{\partial b_m}{\partial \sigma_L} < 0$  (fig. 15), it is  $b_m$ !  $< b_m$ . Under torsional buckling of the stiffeners, the skin forces a different point of rotation than by nonexisting skin and consequently, increases the critical compressive stress substantially. Aside from that, the skin - in flexural buckling as well as torsional buckling - forms an elastic support of the profile, thus effecting a further increase in its buckling load. But the skin may have an adverse effect on local buckling unless skin thickness and profile wall thick-

ness are markedly unlike. For in this case the buckling of the skin invites premature buckling of the profile.

b) Substitution of curved-panel compression test for the full shell-bending test .- In view of the described covering (skin) effects on the buckling process, it seems hardly possible to be able to ascertain the actual buckling stress of the stiffeners by purely mathematical treatment. On the other hand, it is no simple matter to determine the failing-bending moment by bending test on the entire full shell. According to the investigations of the preceding section, the stress condition of the full shell is accounted for by bending; besides, if the skin is buckled, a slight influencing on the buckling stress of the individual stiffeners through the stress condition of the adjacent stiffeners, is to be expected. It is therefore logical for the determination of the failing-bending moment to replace the full-shell bending test by a compression test with a curved panel having a compression zone patterned after the full shell. It reproduces the elusive effect of the skin on the buckling stress of the stiffeners fairly accurately.

One difficulty, however, encountered in curved-panel tests is the correct choice of support conditions and the length of the panel, because the stiffeners in the full shell are more or less elastically restrained, depending

on the type of attachment to the bulkheads and the design of the bulkhead section. If the bulkheads are attached to the skin and the slipped-through stiffeners rigidly connected with them, it approximately resembles full restraint if the bulkheads are tolerably torsion-resistant. But, if only the inner edges of the stiffeners rest on the bulkhead rings not joined to the skin, the stiffeners may turn at the bulkheads. A certain elastic restraint is active in this case also, because on buckling the stiffeners in the adjacent bulkhead sections bend alternately inward and outward and the elastic support of the curved skin in these two directions is different.

In the chosen test arrangement of the panel compression test, as described in II,5,b, the stiffeners are fairly rigidly clamped at the strong angles (figs. 26 to 30). Choosing the length of panel equal to the simple bulkhead cpacing, it approximately corresponds to a full restraint of stiffeners in the full shell. To simulate the case of stiffeners elastically supported at the bulkheads of the full shell with the present panel restraint at the side angles, their length must be equal to twice the bulkhead spacing. But in curved shells this choice of panel length is somewhat too unfavorable on account of the described elastic support due to the skin, and also on account of the possible reciprocal supporting of the stiffener sections in the full shell. The associated elastic restraint and support was allowed for by riveting an intermediate bulkhead piece to the inside of the stiffener sections in the center of the panels of twice the bulkhead spacing.

In order to establish the effect of the length and of the restraint on the load capacity numerically, a series of tests was made with one short and one long panel each in the described manner for five different section designs. The shells had closed-hat sections (figs. 25, 26, and 27), open Z-sections (figs. 28 and 29), and open-hat sections (fig. 30); in two series the section height and in one series the section spacing and the skin thickness were varied in addition. Further data will be found in table I. In the first four series, mean wall thickness sm, skin thickness su, curvature radius r, and section spacing b were alike, thus making the findings of the failing tests available for an evaluation of the best form and height of sections. With this in view, an additional compression test on a very short panel with open-hat sections but otherwise identical dimensions was made. (See table

I, last line.) The distance between the centers of gravity of stiffener attachment bolts served as shell length l.

The identical aspect of failure for both the short and long shell with the higher closed-hat sections (figs. 25, 26, and 27) leads one to the conclusion that the length or restraint in these shells is of secondary importance. These shells failed by starting with strictly local buckling at the flanges on which the length has no effect. From the mean failing stress  $\sigma_{m,B}$  of the panel and the failing stress  $\sigma_{L,B}$  of the stiffeners in table I, it is apparent that the load capacity is the same for the short as for the long shell, but not for shells with low-hat sections.

Then, even the long shell discloses an appreciable drop (13 percent) in load capacity compared to the short shell; and for the long shell with low Z-sections, it is 22 percent less than for the short one. In shells with high Z-sections and open U-channels, the respective drop is 18 and 13 percent for the long shell. This greater drop in the load capacity for open sections is attributable to the form of failure (figs. 28 and 29). These shells fail in buckling accompanied by twisting of the sections being therefore associated with the restraint of the ends of the members. The more pronounced effect on the short shell is seen in figure 28, while the intermediate bulkhead in figure 29 has no appreciable restraining effect on the twisting of the sections of the long shell.

Based upon the compression tests, it may be stated that in shells with stiffener sections which fail through buckling - that is, particularly those with closed (not too compact) hat profiles, the length chosen for the compression test is of no concern, whereas it has a notice—able effect on the load capacity of shells with stiffener sections which fail in flexural and torsional buckling, particularly, those having short open profiles. For such shells the choice of panel length lies between the single and double former spacing, depending on the bond of the stiffeners existing in the full shell.

c) Method of failing - bending moment determination. There are two ways of computing the failing-bending moment by means of the failing stress of the panel from the compression test: First, by computing the mean compression

stress  $\sigma_{m,B}$  of the panel on failing under the assumption of a fully supporting section and multiplying this by the section modulus W of the fully supporting section of the full shell. This gives the bending moment at failure:  $B_k = \sigma_{m,B} W$ . In the second case, we resort to the effective width bm and determine the failing stress oL.B its stiffeners at the instant of failure of the panel, multiplied by the section modulus W' of the full shell with allowance for the unlike effective widths at the individual stiffeners in bending. It gives the ultimate bending moment:  $B_k' = \sigma_{L,B} W'$ . Rather than computing the failing stress  $\sigma_{L,B}$  with the aid of the apparent width, the stiffener stress in the panel test can, of course, also be measured as near to failure as possible, and then extrapolated to failure. The ultimate bending obtained by the first method is lower than that by the second, since only the smallest apparent width existing at the extreme compression fiber of the bent full shell is involved. The first method is therefore on the safer side quite apart from being much more simple since it affords the apparent width direct without making the tedious calculation of the section modulus W' necessary.

The bending moment at failure in bending with transverse load can equally be obtained from a panel test. In a cylinder with restrained end warping (figs. 22 and 23) the compressive stresses of the stiffeners in the full shell ( $\sigma_L + \Delta \sigma_L$ ) due to bending and additional stress through the tension panels (cf. section II,5,d) must not exceed the failing stress  $\sigma_{L,B}$  established in the panel compression test. For the first method the stress  $\Delta \sigma_L$  of the extreme stiffeners must be reduced to the mean failing stress, which then affords as supportable bending moment by simultaneous transverse load:

$$B_{k} = \left(\sigma_{m,B} - \Delta \sigma_{L} \frac{\sum F_{L} + n b_{m} s}{\sum F_{L} + n b s}\right) W$$

where  $\Sigma$  FL is again the total stiffener section and n the number of skin panels. The second method gives at once:

$$B_{k}$$
 =  $(\sigma_{L,B} - \Delta \sigma_{L}) W$ :

Under greater transverse load or different shell-end stiffening, however, the bending loads q may, as a result of the deflected tension bays, stress other stiffeners in the compression zone more unfavorable than the extreme ones. In this case the panel test must include other than the compressive loading a transverse loading. (Cf. section III, 2.)

As a check on the two suggested methods, and for comparison of the ultimate bending moments attainable for different section design but equal weight, a series of bending tests with and without transverse load were carried out on three circular cylinders of the dimensions given in table II. The loading arrangement was the same as for the stress measurements (fig. 19). The photographs of the cylinder failure (figs. 31-34) resemble those for the corresponding panel failure (figs. 25-30), with the exception of the more pronounced deflection of the stiffeners of the full shell with Z-sections (fig. 33) in the first panel in contrast to that of the full shell with open-hat sections (fig. 34). The reason for this is that the first cylinder is stressed in bending with transverse load and consequently, stressed more severely in the first panel than in the others. In this case the first panel is visibly restrained through the second panel which is not loaded to failure.

The ultimate bending moment in the full-shell test measured in pure bending and in bending with transverse load, is given in table II. It is readily apparent that the full shell with open Z-sections supports in bending with transverse load about 10 percent higher bending moment than in pure bending, as the result of the abovementioned restraining effect. In the full shells with hat sections which largely failed in buckling, this restraining effect is of no influence on the failing stress, so that the ultimate bending moments are approximately alike in bending with or without transverse load. The comparison of the cylinders of equal weight discloses the cylinder with closed stiffener profiles to be superior to the other two cylinders with open stiffener profiles as far as bending strength is concerned. The failing stresses om. B and oL, B agree with the values for the relevant panels in table I (series 1, 3, and 5).

On comparing the theoretical and experimental ultimate bending moments, it will be found that the first, simpler method affords sufficiently accurate failing val-

ues for the first two cylinders, but falls short by about 14 percent for the third cylinder. The second method gives the correct value for the third cylinder, but slightly too high values for the other two cylinders when compared with the pure bending figure for the first cylinder. On the other hand, the computed value for bending with transverse load is in agreement with the experimental figure. The reason for the underestimated load capacity of the third cylinder, is due to the greater sectional proportion of the skin (s = 0.5 instead of 0.4 millimeter), as a result of which the incorrectly presumed effective width made itself more noticeable.

2. Failing Strength Under Twisting and

Combined Bending and Twisting

The tension bays under twisting subject the stiffeners of the full shell to compressive loads and distributed radial loads whose support loads must be taken up by the bulkheads. If the bulkheads are sufficiently rigid, the failure may take place through flexural buckling of the stiffeners between the bulkheads. The whole system buckles below a certain bending stiffness of the bulkheads. Lastly, failure may occur through local collapse of the longitudinals or of the bulkheads as, for instance, at the points of load application.

Whether or not the radially loaded bulkheads are stiff enough to force the stiffeners into buckling between the bulkheads, can be ascertained by disregarding the elastic support of the stiffeners due to the skin in the following manner: In order to avoid buckling in the circular plane of a circular ring of radius r under uniform inwardly radial load p, its minimum flexural stiffness must be:

$$EJ_R' = \frac{pr^3}{3}$$
 (reference 30)

To insure Eulerian buckling of the longitudinals between the rings at spacing a in an axially loaded system of members of length  $\boldsymbol{l}$  which, without skin, consists of a number of longitudinals and rings, a minimum bending stiffness of the ring of

$$EJ_{R}^{\dagger} = \frac{\pi}{9} \left( 1 + \cos \frac{\pi a}{l} \right) \frac{r^{3}}{a^{3}} EJ_{L}$$

is required, if EJL is the radial bending stiffness of all stiffeners. The rings in the radially and axially loaded system are rigid enough to force the longitudinals to buckle between the rings if they have a minimum bending stiffness of

$$EJ_R = EJ_R' + EJ_R''$$

Owing to the influence of the skin, the purely mathematical treatment of the buckling-bending strength of the stiffeners in twisting is beset with the same difficulties as the determination of its buckling strength under bending. But here also, it is possible to obtain the buckling strength with allowance for skin effect from panel tests. The panels are then to be simultaneously stressed under the axial compression L and a lengthwise distributed transverse load Q. The loads to be taken up by the stiffeners alone are obtained from the tension-bay theory. (Cf. section II, 5, e.) The choice of panel length follows the same arguments as for the pure compression test (cf. section III, 1, b), although for panels of double bulkhead spacing the intermediate bulkhead must be support to take the bearing pressure of the transverse load. The load ratio  $\lambda = L/Q$  depends on the wrinkling angle  $\alpha$  and consequently, on the load stage &, that is, the ratio of effective twisting moment T to the twisting moment  $T_0$ at the instant of buckling of the skin. This means that λ must be modified continuously in the test as the panel load is increased. If  $\delta_B$  is the load stage at failure, then the sought-for critical twisting moment becomes:  $T_B = \vartheta_B T_0$ . If the buckling load has been exceeded considerably (8 > 10), it is advisable to compute the load ratio  $\lambda$  on the assumption of a complete tension bay; if little exceeded, by assuming an incomplete tension bay. With complete tension bays the respective loads L and Q apportioned to a stiffener between two bulkheads of spacing a, are:

L = b s 
$$\sigma_n$$
 = b s  $(\tau \cot \alpha + \sigma_2)$   
Q =  $\frac{a}{r}$  b s  $\sigma_u$  =  $\frac{a}{r}$  b s  $(\tau \tan \alpha + \sigma_2)$ 

or, with  $\sigma_2$  omitted:

$$\lambda = \frac{r}{a} \cot^2 \alpha$$

To appraise the discussed calculation method as well as to compare several designs of the same weight, the cylinders compiled in table II were subsequently subjected to twisting tests. The loading was effected on the same test rig (fig. 19), the device for applying a pure twisting moment being shifted 90°. Figures 35-37 illustrate the failures of the three investigated cylinders. In every case the stiffeners failed in flexural buckling. On the cylinder with Z-sections (fig. 35), it was accompanied by twisting of these sections; on the cylinder with closed-hat profiles (fig. 36), by local buckling of the channel flanges; and in the last cylinder (fig. 37), by spreading or contraction of the open-hat profiles accompanied by buckling of the back of the profile. The recorded critical twisting moments are compiled in table III. Of the three shells of identical weight, the one with closed profiles manifested under twisting - much more even than in bending the greatest load capacity.

On comparing the theoretical and experimental critical twisting moments of the second and third cylinders, it is found that the premise of complete tension bay affords a good agreement between theory and test for the thin-walled cylinder (0.4 mm) stiffened with closed-hat profiles, while the calculation evolved on the basis of the complete tension bay for the cylinder of 0.5 mm thickness and open-hat profiles, falls short by about 14 percent and is too high by 8 percent for the incomplete tension bay. The compression-bending tests on the panels patterned after the second and third cylinders were made for a shell length equal to single bulkhead spacing; the ends of the panels were clamped in the rigid angles (figs. 25-30) as in the compression test. This arrangement is somewhat too favorable for panels with open-hat profiles for reasons given in III, 1, b (cf. table V, column 5), which explains the discrepancy between theory and test of the third cylinder by complete tension bay.

The cylinders given in table II were subsequently tested under combined bending and twisting for different B/T ratios. Figure 38 illustrates the failure of such a test. The B and T values existing at the instant of failure are shown in figure 39, plotted against the respective failing moments Bo and To of different cylinders in pure bending and pure twisting. Apart from the test point of cylinder III, the others lie on or between the plotted curves:

$$\frac{B}{B_0} = 1 - \left(\frac{T}{T_0}\right)^n \quad \text{for } n = 2 \quad \text{and} \quad n = 3$$

Accordingly, with predetermined failing moment in pure bending and pure twisting, it is approximately possible to predict the failing moments for combined bending and twisting. The departure of the test point of cylinder III is due to the fact that this cylinder was subject to a greater preliminary stress than the others.

In view of the scarcity of experimental data, the method should be applied with some caution.

## 3. Effect of Section Design on the Compressive Strength

Since, in view of the discussed experiments, the load capacity of a full shell stressed in bending, is primarily contingent upon the compressive strength of its compression zone, it is possible to ascertain the best sectional design of the shell for equal weight on the basis of panel compression tests. For this purpose a large number of tests were made in the DVL, of which table III gives some typical results.

The individual groups of panels differ in circumferential weight distribution, for which the mean wall thickness sm serves as criterion; panel curvature and length in the different groups were also unlike. The distribution of the section over skin and stiffeners was also varied. The most important result of the compression tests is the following: The greater the cross-sectional proportion of the stiffeners ( $F_{
m L}/{
m b}$ ) the greater the load capacity of the shell given through the mean failing stress. The smaller the mean wall thickness sm, the more pronounced the difference in shell load capacity with greater or lesser share of the stiffeners. So from the point of view of static strength, it is advisable - particularly, with the thin shells usually employed as shell bodies to strive for minimum skin thickness, in order to attain strongest possible stiffeners with high buckling stresses. Heavy shells, less frequent as shell bodies than as shell wings, are, on the other hand, less responsive to crosssectional distribution. Increasing the stiffener spacing of thin shells, should enhance the load capacity; this, while it would somewhat lower the load capacity of the skin, would, on the other hand, benefit the load capacity of the stiffeners, which then could be designed to resist

buckling and bulging to a greater extent, so long as the failing strength of these stiffeners does not come too close to the yield point. But the stiffener spacing is upwardly limited insofar as no bulging of the skin is permissible under operating condition. A fifth or sixth of the failing load is usually considered the lower limit for the bulging load of the skin. To this must be added, if the shell has a marked curvature, that wide stiffener spacing promotes comparatively deep wrinkles.

The whole test series attests to the extent of attainable failing strength with increasing mean wall thickness. The rise is substantially slower in the range of greater s<sub>m</sub>, because the failing stress of the stiffeners gradually approaches the yield point, beyond which no further increase is possible. The effect of section form is seen from a comparison of the series 1, 3, 5 of group 1, with series 1 and 3 of group 2; however, it must be borne in mind that in longer shells the differences in failing strength of shells with open and closed profiles become even greater. (Cf. table I.)

The effect of shell curvature already apparent from the last columns of table III, was separately investigated on three different shell forms (fig. 40) and sm = 0.75 mm mean wall thickness. From the test data it becomes apparent that increasing the curvature of the skin of thinwalled (0.4 mm) shells with open profiles, does not increase the load capacity. Contrariwise, the same shells (of 0.4 mm wall thickness) but with closed profiles, as well as the thicker shells (0.5 mm) with open profiles, disclose a greater rise in failing stress. The explanation for this lies with the greater effective width of the skin of the last two shells. The ensuing greater load absorption of the skin makes its curvature more noticeable than before. The three tests of the second series were made under the following conditions: The stiffeners of the first shell rested only partially on the angles, while in the other two shells the stiffeners rested throughout on the angles. The experiments bring out the effect of the different load applications.

From the greater rise in load capacity of the shells with thicker walls by increasing curvature, it follows that the equivalence of thick-walled shells of shallow curvature, with respect to such with thin skin and greater curvature, is reached so much sooner under increasing circumferential load  $p=s_m\ \sigma_{m.\,B}$  as the shell curvature

is greater. Wagner (reference 31) gives as decisive limit value:  $\frac{p}{r} = 25 \text{ kg/cm}^2$ , which value is approximately reached by the more curved shell in the last column of table III  $\left(\frac{p}{r} = 19 \text{ kg/cm}^2\right)$ .

In conclusion, we give the result of some studies on the effect of profile beading on the failing strength (table IV). The test panels were of equal mean wall thickness ( $s_m = 0.75 \text{ mm}$ ) curvature radius, length of shell and spacing; the stiffeners were Z-sections of 0.79 mm thickness in the first, and of 1.20 mm wall thickness in the other group, the stiffeners of the first group being 1) beaded on both flanges, 2) at the flange touching the skin, 3) only at the flange not touching the skin, and 4) plain flanges without beading.

In the second group, both flanges were beaded and then left plain (without beading). The result expressed in terms of mean failing stress is to the effect that in the thin-walled sections of the first group, especially the bead on the skin side, is important; a shell with such beaded sections has the same load capacity as the shell with section beaded on both sides. The shell with section beaded on the non-touching flange can carry no greater load than the shell with plain (not beaded) sections. The bead in such shells has the important task of protecting the section against bulges of the skin which otherwise promote premature bulging of the thin-walled stiffeners.

In contrast with this, the shell with thick-walled stiffeners manifests no substantial effect of the beading. The panel fails in lateral buckling accompanied by twisting of the stiffeners. This precludes premature bulging due to skin wrinkles. As concerns the tendency of the stiffeners to bulging through the skin, the rivet spacing is also without influence.

Translation by J. Vanier,
National Advisory Committee
for Aeronautics.

## REFERENCES

- l. Winter, H., and Hoffmann, E.: Zusammenstellung von konstruktiven Einzelheiten ausgeführter Glattblechschalenrumpfe des Auslandes. Luftfahrtforschung, vol. 11, no. 8, February 6, 1935, pp. 235-240.
- 2. Flügge, Wilhelm: Statik und Dynamik der Schalen. J. Springer, Berlin, 1934.
- 3. Goodey, W.: Thin Sections in Torsion. Aircraft Engineering, London, December 1936, pp. 331-334.
- 4. Wagner, H., and Simon, H.: Über die Krafteinleitung in dunnwandige Zylinderschalen. Luftfahrtforschung, vol. 13, no. 9, 1936, pp. 293-308.
- 5. Reissner, H.: Neuere Probleme der Flugzeugstatik.
  Z.F.M., vol. 17, no. 18, September 28, 1926, pp.
  384-393.
- 6. Ebner, Hans: Torsional Stresses in Box Beams with Cross Sections Partially Restrained against Warping. T.M. No. 744, N.A.C.A., 1934.
- 7. Flügge, W.: Die Stabilität der Kreiszylinderschale. Ing. Arch., vol. 3, 1932, pp. 463-506.
- 8. Geckeler, J. W.: Plastisches Knicken der Wandung von Hohlzylindern und einige andere Faltungserscheinungen an Schalen und Blechen. Z.f.a.M.M., vol. 8, no. 5, October 1928, pp. 341-352.
- 9. Donnell, L. H.: A New Theory for the Buckling of Thin Cylinders under Axial Compression and Bending.
  Trans. A.S.M.E., vol. 56, no. 11, 1934, pp. 795-806.
- 10. Timoshenko, S.: Theory of Elastic Stability. McGraw-Hill Book Co., New York, 1936, p. 467.
- 11. Redshaw, S. C.: The Elastic Instability of a Thin Curved Panel Subjected to an Axial Thrust, Its Axial and Circumferential Edges Being Simply Supported.
  R. & M. No. 1565, British A.R.C., 1934.
- 12. Dschou, Dji-Djuan: Die Druckfestigkeit versteifter zylindrischer Schalen. Luftfahrtforschung, vol. 11, no.
  8, 1935, pp. 223-234.

- 13. Heck, O. S.: The Stability of Orthotropic Elliptic Cylinders in Pure Bending. 1937.
- 14. Heck, O. S., and Ebner, Hans: Methods and Formulas for Calculating the Strength of Plate and Shell Constructions as Used in Airplane Design. T.M. No. 785, N.A.C.A., 1936.
- 15. Ballerstedt, H. and Wagner, H.: Versuche über die Festigkeit dunner unversteifter Zylinder unter Schubund Langskräften. Luftfahrtforschung, vol. 13, no.
  9, 1936, pp. 309-312.
- 16. Lundquist, Eugene E.: Strength Tests on Thin-Walled Duralumin Cylinders in Torsion. T.N. No. 427, N.A.C.A., 1932.
- 17. Bridget, F. J., Jerome, C. C., and Vosseller, A. B.:

  Some New Experiments on Buckling of Thin-Wall Constructions. Trans. A.S.M.E., vol. 56, no. 8, 1934,
  pp. 569-578.
- 18. Marguerre, K., and Trefftz, E.: Über die Tragfähigkeit eines langsbelasteten Plattenstreifens nach Überschreiten der Beullast. Z.f.a.M.M., April 1937.
- 19. Marguerre, K.: Die mittragende Breite der gedrückten Platte. Luftfahrtforschung, vol. 14, no. 3, March 20, 1937, pp. 121-128.
- 20. Lahde, R., and Wagner, H.: Experimental Studies of the Effective Width of Buckled Sheets. T.M. No. 814, N.A.C.A., 1936.
- 21. Newell, Joseph S.: Skin Deep. Aviation, vol. 34, no. 11, 1935, pp. 19-20; and no. 12, pp. 18-20.
- 22. Kromm, A.: Einfluss der Nietteilung auf die Druckfestigkeit versteifter Schalen aus Duralumin. Luftfahrtforschung, vol. 14, no. 3, March 20, 1937, pp. 116-120.
- 23. Wagner, Herbert: Flat Sheet Metal Girders with Very Thin Metal Web.

Part I - General Theories and Assumptions. T.M. No. 604, N.A.C.A., 1931.

(Continued on p. 48a)

## REFERENCES (Cont.)

- Part II Sheet Metal Girders with Spars Resistant to Bending Oblique Uprights Stiffness. T.M. No. 605, N.A.C.A., 1931.
- Part III Sheet Metal Girders with Spars Resistant to Bending The Stress in Uprights Diagonal Tension Fields. T.M. No. 606, N.A.C.A., 1931.
- 24. Wagner, H., and Ballerstedt, W.: Tension Fields in Originally Curved, Thin Sheets During Shearing Stresses. T.M. No. 774, N.A.C.A., 1935.
- 25. Schapitz, E.: Über die Drillung dunnwandiger, versteifter Kreiszylinderschalen. Jahrb. Lillienthal Ges. f. Luftfahrtforschung, 1936, p. 94.
- 26. Lahde, R., and Wagner, H.: Tests for the Determination of the Stress Condition in Tension Fields. T.M. No. 809, N.A.C.A., 1936.
- 27. Schapitz, E.: Contribution to the Theory of Incomplete Tension Bay. T.M. No. 831, N.A.C.A., 1937.
- 28. Schapitz, E.: Jahrb. Lillienthal Ges. f. Luftfahrtforschung, 1936.
- 29. Lahdo, R., and Wagner, Herbert: Experimental Studies of the Effective Width of Buckled Sheets. T.M. No. 814, N.A.C.A., 1936.
- 30. Handbuch der Physik, vol. 6, p. 286.
- 31. Wagner, Herbert: Überblick über die Probleme der Schalenfestigkeit. Luftwissen, December 1935.

Table I Effect of length of panel, of profile form and height on the load capacity in compression.

0	$s_m=0,75$ ;	$s_H = 0.4;$ $s_H = 0.5;$	$b = 140 \\ b = 210$	; $r = 400$ mm at s	mm. eries 5
Seri	Section	l	i	$\sigma_{m,B}$	O'L,B
S	20001014	mm	mm	. kg/cm²	kg/cm²
1	074	340	7,1	1320	1820
	274	700	7,1	1300	1880
2	22	340 700	4,9 4,9	1210 1055	1830 1590
3		340 700	6,4 6,4	1220 950	1840 1500
4	70 8	340 700	7,6 7,6	1430 1175	2370 1950
5		340 700	7,5 7,5	980 860	1850 1650
6	975	340	7,5	1140	1760

Table IV Effect of section bead on the load capacity of panels in compression.

	-					
$s_m = 0.75$	r =	= 400	l = 340	b = 140 [mm	1]	
Stiffeners	Skin thick- ness	Wall thick - ness of stiffener	Mean fail- ing Stress	Type of	faile	ire
-	mm	mm	kg/cm²	_		
	0,35	0,79	850	Collapse	of	flange
	0,35	0,79	860	"		,,
73.5	0,35	0,79	650	.,	*,	**
777	0,35	0,79	670			" .
78	0,40	1,20	990	Bulging	and	twisting
	0,40	1,20	920	"	11	

Table II

Buckling and failing moment in bending and torsion, theoretical and experimental.

Cyl- in- der No.	Section s	ketch	Bending mo- ment under buck- ling of skin	Means stro of ponel	ess	Compo	e bending of full surfed wing to $B_{k'} = \sigma_{L,n}W'$	Meas		ing mo- ment on buck- ling of	Com	ent of shell puted Incom plete	full for   meas-   ured
Nr.			kgem	kg/cm²	kg/cm <sup>2</sup>	kgem	kgem	kgcm	kgem	kgem	kgem	kgem	kgcm
I	140 -14-15 Regular	Section F = 18.7cm <sup>2</sup> Section modulus for: fully supporting skin W = 367cm <sup>3</sup> partially supporting skin W' = 255cm <sup>3</sup>	62 700	950	-1500	350 000	380 000	347 000	380 000 (Q == 1450kg)	31 200			198 500
Ш	140 00 12 0 200 19	Section F = 18.2cm <sup>2</sup> Section modulus for: fully supporting skin W = 356cm <sup>3</sup> partially supporting skin W = 279cm <sup>3</sup>	66 800	1320	-1820	484 000	508 000		497 000 (Q = 1870kg)	22 200	310 000	318 000	307 000
IV	200 Runn War War	Section F = 18.7cm <sup>2</sup> Section modulus for: fully supporting skin W = 367cm <sup>3</sup> partially supporting skin W = 243cm <sup>3</sup>	89 000	850	-1650	340 000	405 000		407 000 (Q = 1530kg)	53 400	198 000	250 000	231 000

N.A.C.A. Technical Memorandum No.

Table III

Effect of section distribution on the load capacity of panels in compression.

Rodius length	Section	Mean wall thickness	Skin thickness	Section pro- portion of Stiffeners	Spacing	Buckling stress	Mean fail-	
rerigin		8111	8	FL/b	b :	377633	ing stress	of stiffeners
*		mm	mm	mm	mm	kg/cm²	kg/cm²	kg/cm²
= 340	1,12 %	0,75	0,4	0,35	140	210	1220	1840
= 7	205 %	0,75	0,6	0,15	140	290	630	1010
	5 2,75 3	0,75	0,4	0,35	140	210	1140	1760
= 400	J- 975 8	0,75	0,5	0,25	210	250	980	1850
, = 'r	20,74 0	0,75	0,4	0,35	140	230	1320	1820
0	12703 2	1,1	0,55	0,55	104	500	1910	2600
= 300	20,70 %	1,1	0,70	0,40	104	1000	1400	1510
7	103 2	1,1	0,50	0,60	104	430	1630	2000
	J-103 %	1,1	0,75	0,35	156	665	1230	1600
r = 300	7-32-75 25	2,3	0,50	1,80	104	830	2450	2750
	-187 e	2,3	1,50	0,80	104	2200	2230	2330
= \infty = \infty = 425	35-15 13	2,7	1,0	1,70	105	720	2020	2400
= 2	50-	2,7	1,2	1,50	140	800	1880	2200

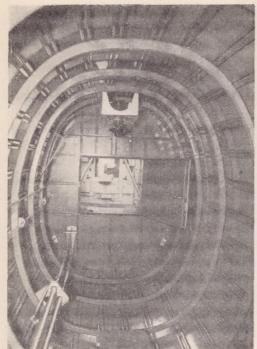


Figure 1.- Heinkel type shell body.

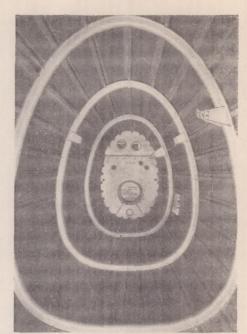


Figure 2.- Henschel type shell body.

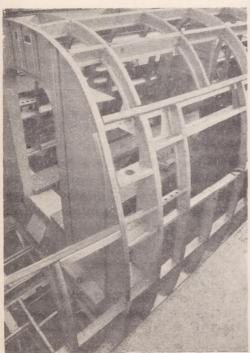


Figure 3.- Center section with main bulkhead of a Heinkel type shell body.



Figure 4.- Heinkel shell body showing cabin.

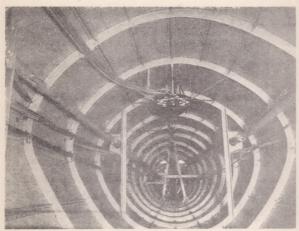


Figure 7.- Dornier type shell body.

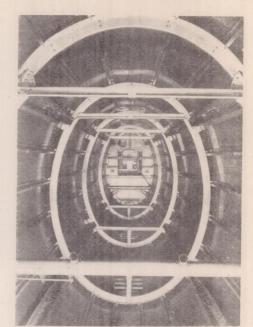


Figure 6.- Junkers type shell body with four reinforced stiffeners.



Figure 5.- Junkers type shell body.

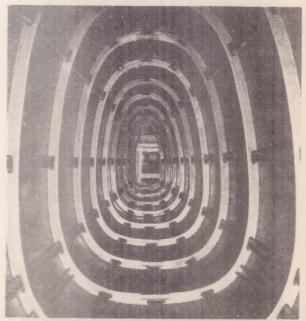


Figure 8.- BFW type shell body.

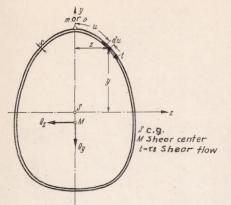


Figure 9.- Section of a plain shell (no stiffeners).

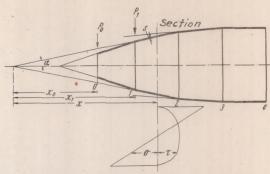


Figure 10.- Sectional view of stress distribution in a

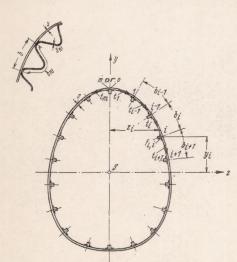


Figure 11.- Shell with stiffeners (symbols).

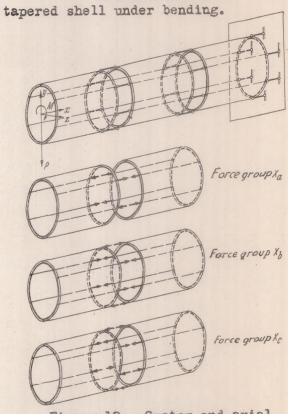


Figure 12.- System and axial load groups X in a two-way stiffened shell with 6 flanges.

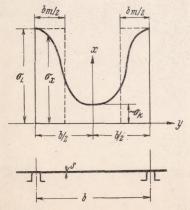


Figure 14 .- Effective width.

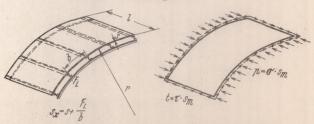


Figure 13.- Stiffened panel under compression and shear.

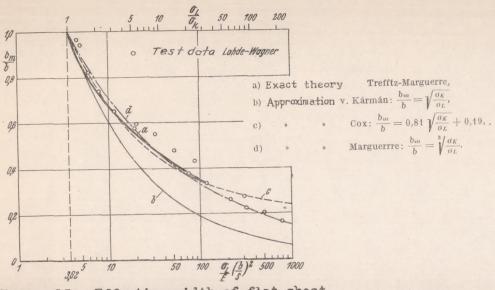


Figure 15.- Effective width of flat sheet according to test and various theories.

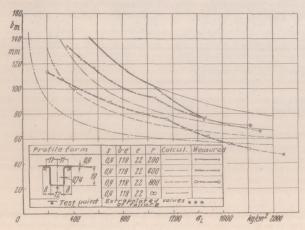


Figure 18.- Computed and recorded effective width of curved sheet with closed-channel stiffeners.

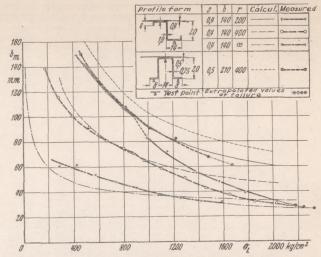


Figure 17.- Computed and recorded effective width of curved sheet with open stiffeners.

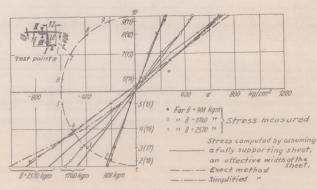


Figure 20.- Computed and recorded stresses of a circular cylinder in pure bending.

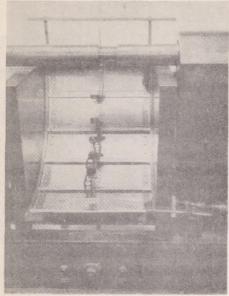


Figure 16.- Panel with clamping angles and test stations.

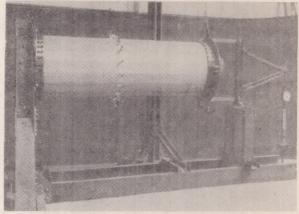


Figure 19.- Rig for testing a circular cylinder under pure bending.



Figure 21.- Wrinkling under bending with transverse load.



Figure 24. - Wrinkling under twist.

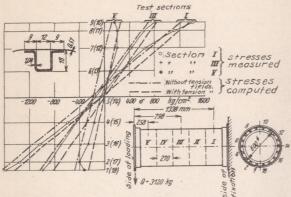


Figure 22.- Computed and recorded stresses on different cross sections under bending with transverse load.

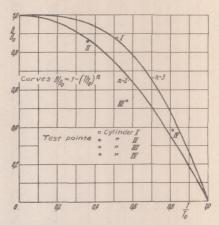


Figure 39.- Proportions of the failing moments under bending and twist.

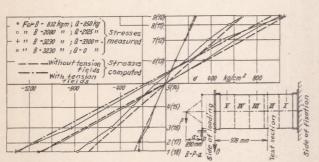


Figure 23.- Computed and recorded stresses in cross section I under bending with transverse load and under pure bending at different load stages.

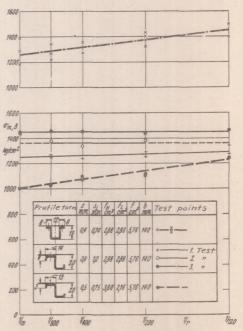


Figure 40.- Mean failing stress of panels versus curvature.



Figure 25.- Failure of panel with closed-hat channels under compression (inside view).



Figure 26.- Failure of panel with closed-hat channels under compression (outside view).

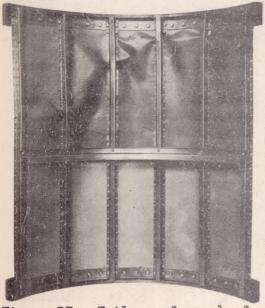


Figure 27. - Failure of panel of double length and closed-hat channels under compression.

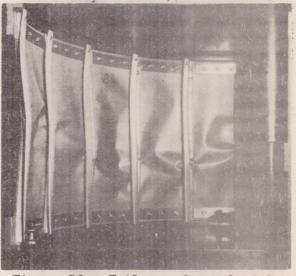


Figure 28.- Failure of panel with Z-sections under comp.

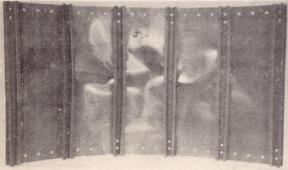
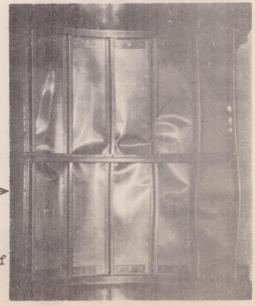


Figure 30.- Failure of panel with open-hat channels under compression.

Figure 29.- Failure of panel of double length and Z-sections under compression.



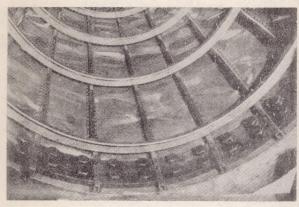


Figure 31.- Failure of full shell with closed-hat channels under bending with transverse load (inside view).

Figure 32.- Failure of full shell with closed-hat channels under bending with transverse load (outside view).



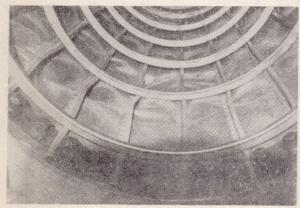
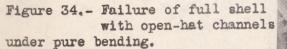


Figure 33.- Failure of full shell with Z-sections under bending with transverse load.



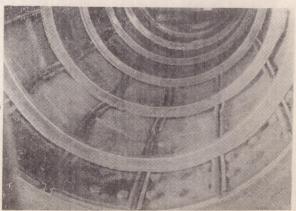




Figure 35.- Failure of full shell with Z-sections under pure twist.

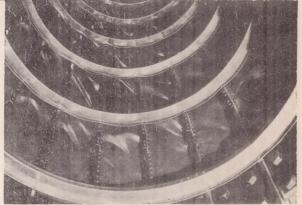


Figure 36.- Failure of full shell with closed-hat channels under pure twist.

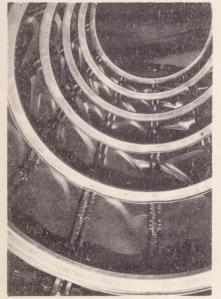


Figure 37.- Failure of full shell with open-hat channels under pure twist.

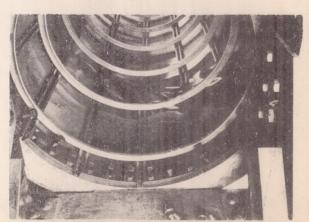


Figure 38.- Failure of full shell with open-hat channels under bending and twist.